universität wien

MASTERARBEIT

Titel der Masterarbeit

„Exploring the molecular basis for different EB1 interaction networks in budding yeast“

verfasst von

Josef Fischböck Bsc

angestrebter akademischer Grad

Master of Science (MSc)

Wien, 2014

Studienkennzahl lt. Studienblatt:	A 066 834
Studienrichtung lt. Studienblatt:	Molekulare Biologie
Betreut von:	Dr. Stefan Westermann

Acknowledgments

First I would like to thank Dr. Stefan Westermann for giving me the chance to work in his lab and the scientific guidance during this project.

I would also like to express my gratitude towards all Westermann lab members for being always helpful, inspiring discussions and spending time together in a nice and creative atmosphere. A special thank goes to Dr. Christine Mieck for showing me a lot of different techniques and for always adding some nice scientific input.

Furthermore, I thank Dr. Babet Van der Vaart, my supervisor, for giving me this nice project and her constant and enourmos support.

Finally, I thank my parents for their patience and the great and permanent support I received during my studies.

Zusammenfassung

Mikrotubuli sind essentiell für viele Prozesse in der Zelle, z.B. der akkuraten Aufteilung von Chromosomen, wo Fehler zu ernsthaften Krankheiten wie Krebs führen können. Sie sind intrinsisch polare, höchst dynamische, zylindrische Polymere, welche aus α und β Tubulin zusammengesetzt sind. Während die plus Enden dynamisch sind und zwischen Wachstums-Perioden und Depolymerisation wechseln, sind die Minus Enden bevorzugt verankert an den Zentrosomen. Die Dynamik von Mikrotubili ist in lebenden Organismen durch Mikrotubuli assoziierte Proteine (MAPs) reguliert. Mutationen in Genen, die für diese Klasse von Proteinen codieren, können zu Defekten in der Entwicklung der Großhirnrinde führen. Eine Untergruppe von MAPs sind die +TIPs, welche aktiv am plus Ende von Mikrotubuli lokalisiert sind, was sie in eine perfekte Position bringt, um sowohl die Dynamik von Mikrotubuli als auch deren Befestigung an zelluläre Strukturen wie die Zellwand, Kinetochore, endoplasmatisches Retikulum zu kontrollieren. In den letzten Jahren verdeutlichten sich die Anzeichen, dass Proteine der EB-Familie eine zentrale Rolle in der Etablierung von Proteinnetzwerken an den Mikrotubul Plus Enden einnehmen, in dem sie andere +TIPs dort hin rekrutieren. EB Proteine besitzen eine EBH Domäne, durch welche sie mit Proteinen, welche ein SxIP (Serin – beliebige Aminosäure –Isoleucin – Prolin) Motiv besitzen, Bindungen eingehen können. Zusätzlich können EB Proteine über ihren sauren/aromatischen C-Terminus mit den basischen Domänen in CAP-Gly Domänen enthaltenden Proteinen wie CLIP-170 und p150glued/Dynactin interagieren. EB Proteine sind hoch konserviert und wohingegen in Säugern drei Mitglieder der EB Familie existieren (EB1, EB2 und EB3), gibt es in dem simplen Modellorganismus Hefe nur ein Homolog namens Bim1. In dieser Arbeit untersuchte ich die molekulare Grundlage für verschiedene, auf EB1 basierende Interaktions-Netzwerke durch Verwendung von Hefe, welche die kombinierte Anwendung genetischer, biochemischer und zellbiologischer Methoden ermöglicht. Ich generierte Mutanten, die die Interaktion mit Proteinen, welche SxIP Motive und/oder CAP-Gly Domänen enthalten, verhindern. Durch den Einsatz von „Pull-down“ Experimenten gefolgt von Massenspektrometrie wurde die Komposition von Proteinen, die mit diesen Bim1 Mutanten assoziieren, bestimmt.

Die Bim1 Mutante in der beide Domänen mutiert waren, ermöglichte es die spezifischen Effekte von Bim1, unfähig mit Bindungspartnern zu interagieren, auf die Regulation des Mikrotubuli Zytoskeletts zu untersuchen. Der Phänotyp dieser Mutante wurde durch Mikroskopie an lebenden Zellen und Viabilitätstests determiniert. Dadurch konnte ich zeigen, dass eine Bim1 Mutante, die nichtmehr mit ihren Bindungspartnern interagiert, ähnliche Phänotypen (Wachstums Defekte, Miss-Orientierung der Spindel) hat wie ein Stamm, in dem Bim1 deletiert ist.

Zusätzlich dazu identifizierte ich Ase1, das PRC1 Homolog, welches antiparallele Mikrotubuli bündelt, als neuen Bim1 Interaktionspartner und charakterisiere die Bindung zwischen den beiden durch eine Kombination von biochemischen und auf Mikroskopie basierten Methoden. Damit konnte ich zeigen, dass in lebenden Organismen der N-Terminus von Ase1 und die EBH Domäne von Bim1 für die Interaktion zwischen den beiden benötigt werden.

Abstract

Microtubules are central to many essential processes in cells, such as accurate chromosome segregation, where alterations can lead to severe diseases like cancer. They are intrinsically polar, highly dynamic, cylindrical polymers of α/β-tubulin heterodimers. While the plus ends are the dynamic ends of microtubules that switch between periods of growth and shrinkage, the minus ends are preferably anchored at the centrosomes and have a much lower net exchange rate of tubulin dimers. In vivo, microtubule dynamics are regulated by microtubule-associated proteins (MAPs). Mutations in genes, encoding for this class of proteins, can cause defects in the development of the cerebral cortex. A subgroup of MAPs, the plus-end tracking proteins (+TIPs), actively remain at growing microtubule plus ends. They are not only perfectly positioned to control microtubule dynamics, but they also serve as a link between the microtubule network and cellular structures (i.e. cell cortex, kinetochores, endoplasmatic reticulum).

In the recent years the End Binding (EB) protein family has emerged as central adaptors of microtubule tip associated networks, as EBs can recruit other +TIPs to growing microtubule ends. EB proteins contain an EB homology (EBH) domain, which allows them to interact with SxIP (serine – any amino acid – isoleucine – proline) motif containing proteins. In addition, EB proteins can interact via their acidic/aromatic C-terminus with the basic groove of CAP-Gly domain containing proteins, such as CLIP-170 and p150glued/dynactin. EB proteins are highly conserved and whereas mammals contain three EB family members (EB1, EB2 and EB3) in the simple model organism *Saccharomyces cerevisiae* (budding yeast) there is only one homologue called Bim1. Here I investigated the molecular basis for different EB1-based interaction networks by using budding yeast, which is highly amenable to the combined application of genetic, biochemical and cell biological studies.

I generated mutants abrogating the interaction with SxIP motif and/or CAP-Gly domain containing proteins. By performing pull-down assays followed by mass spectrometry the composition of +TIPs associated with these Bim1 mutants was determined.

The Bim1 mutant that had both interaction domains mutated simultaneously, allowed me to dissect the specific roles of Bim1, unable to bind any partners, on the regulation of the microtubule cytoskeleton. The phenotypes of the mutant strains were determined by live cell imaging of fluorescently tagged proteins using Deltavision Deconvolution Microscopy and by performing benomyl spot assays. These experiments clearly demonstrated that the Bim1 mutant, unable to bind to interaction partners, phenocopies a Bim1 deletion strain (growth defects, spindle misorientation, “spindle rocking”).

In addition to that, I identified the PRC1 homologue Ase1, which bundles antiparallel microtubules, as a novel binding partner of Bim1 and I further characterized this interaction

by performing a combination of biochemical and microscopy-based assays. I could show that in vivo the interaction between Ase1 and Bim1 depends on the N-terminal part of Ase1 and the EBH domain of Bim1.

List of contents

1. Introduction 1

1.1 Microtubules 1

1.2 Microtubule associated proteins 3

1.3 +TIPs 6

1.4 EB proteins 7

1.5 Bim1 10

2. Aims of my project 10

3. Materials and Methods 12

3.1 Yeast strain construction 12

3.2 In vivo FLAG-pull downs from yeast extracts 12

3.3 Mass spectrometry 12

3.3.1 Sample preparation 12

3.3.2 NanoLC-MS Analysis 13

3.3.3 Data Analysis 13

3.4 Purification of GST-tagged Bim1$^{YE/AA}$ from *E. coli* 14

3.5 Purification of FLAG-Ase1-HALO from yeast extracts 14

3.6 Purification of Ase1-STREP variants from SF9 insect cells 15

3.7 In vitro binding assays for different Ase1 and Bim1 variants 16

3.8 MT cosedimentation assay of Ase1-WT and Ase1ΔN 16

3.9 Live cell imaging 16

3.10 TIRF microscopy 17

3.10.1 Labelling of Ase1 with Alexa 594 17

3.10.2 Assembling of flow chambers for TIRF microscopy 17

3.10.3 TIRF microscopy using taxol stabilised MTs 18

3.10.4 TIRF microscopy using dynamic MTs 18

3.11 Size exclusion chromatography (SEC) 19

4. Results 22

4.1 Identification and characterization of EB1 interaction partners using different EB1 mutants in budding yeast 22

4.1.1 Description of the N-terminally tagged Bim1 binding mutants 22

4.1.2 Testing cargo interactions of mutant Bim1 variants 24
4.1.3 Identification of proteins that associate with the N-terminally tagged binding mutants of Bim1 24
4.1.4 Determining the phenotype of N-terminally tagged Bim1 cargo binding mutants 26
4.1.5 Identification of proteins that associate with the C-terminally tagged binding mutants of Bim1 28
4.2 A Bim1 mutant, unable to bind to interaction partners, shows similar phenotypes as a Bim1 deletion strain 30
4.2.1 Growth defect analysis by spot assays 30
4.2.2 Determination of the phenotype of a cargo deficient Bim1 mutant by live cell imaging 31
4.2.3 The cargo deficient Bim1 mutant has an increased doubling time 33
4.3 Detailed analysis of selected Bim1-Cargo interactions 34
4.3.1 Interaction between Bim1 and Nup159 34
4.3.2 Interaction between Bim1 and Bck1 35
4.4 Interaction between Bim1 and Ase1 36
4.4.1 The N-terminal domain is required for proper Ase1 function in vivo 38
4.4.2 Investigating the interaction between Ase1 and Bim1 in vitro 38
4.4.3 Purification of Ase1 from yeast cells and insect cells 39
4.4.4 Ase1 purified from insect cells binds MTs in a cosedimentation assay 40
4.4.5 Ase1 directly interacts with Bim1 via the EBH domain 40
4.4.6 The N-terminal region of Ase1 is not required for binding to Bim1 in vitro 41
4.4.6 TIRF microscopy analysis of Ase1 and Bim1 43
4.4.7 Bim1 promotes recruitment of Ase1 to taxol-stabilized microtubules in vitro 44
4.4.8 Ase1 binds preferentially to microtubule bundles 45
4.4.9 Analysis of Ase1 and Bim1 in combination with dynamic microtubules 46
4.4.10 Ase1 and Bim1 localize independently from each to the spindle midzone 47
5. Discussion 49
5.1 Comparison of different tagging strategies for Bim1 49
5.2 Phenotypes of a cargo deficient Bim1 mutant 50
5.2.1 Spindle positioning defect 50
5.2.2 Effects on microtubule dynamics 51
5.3 Bim1 and Ase1 interaction interfaces 52
5.4 Function of the interaction between Ase1 and Bim1 in vivo 53
6. Table of figures 56

7. Abbreviations.....57

8. References.....58

Curriculum Vitae.....66

1. Introduction

A typical adult human body contains 206 bones, which form the skeletal system and are necessary to fulfil a variety of different functions. Without these bones we simply would not be viable. Analogous to the human body every single cell also requires structures that provide mechanic stability. These structures are formed by the cytoskeleton. Even prokaryotes (cells without a nucleus) have proteins that form a cytoskeleton. These evolutionary fundamental proteins not only provide a scaffold for maintaining the cellular shape, but also play important roles in a number of other processes like intracellular transport, cell division and organelle positioning.

1.1 Microtubules

Microtubules (MTs) are one of the three types of cytoskeletal filaments and are present in all eukaryotes. They are crucial for a lot of different processes in cells. By being part of the axoneme of cilia and flagella, microtubules contribute to cell motility. In addition to that, they help to maintain cell shape and are required to establish cell polarity. By serving as “railway tracks”, MTs play a key role in the intracellular transport of organelles (vesicles, nucleus, endoplasmatic reticulum, Golgi, peroxisomes, mitochondria). During cell division, MTs form the mitotic spindle, which is indispensable for proper chromosome segregation. The effect of MTs on cell migration remains less clear, but they are definitely implicated in this process [1].In order to perform these different kinds of functions, the MT cytoskeleton has to undergo constant remodelling, which is achieved by the constant assembly and disassembly of its subunits [2 3].

Alpha and β tubulins, tightly bound together by non covalent bonds, form heterodimers which are the subunits that build up MTs (Fig. 1A). Longer, linear assemblies of these dimers, so called protofilaments, are linked together laterally (Fig. 1B thus forming a hollow tube with a diameter of 25 nm. In vivo this cylindrical structure typically comprises 13 parallel protofilaments. Protofilaments can laterally associate with to each other in two ways, generating a so called A- (consists of α-β contacts) or B-lattice (made of α-α or β-β contacts) [4]. The predominant type is the B-lattice [5]. The discontinuity in the surface of the MT wall that arises, when 13 protofilamts are forming a hollow cylindrical tube, is known as the MT seam (Fig. 1B). This structure has been implicated to be important for binding of proteins like Mal3p, the *S. pombe* EB1 homolog, to the MT lattice [6].

As α and β tubulin heterodimers are always arranged in a head-to-tail fashion, MTs are intrinsically polar. Alpha tubulin is always at the minus end, which is preferably anchored at the centrosomes, while β tubulin is exposed at the plus end, which is the more dynamic end of MTs that can switch between periods of growth and shrinkage [7], a feature termed dynamic instability (Fig. 1C).

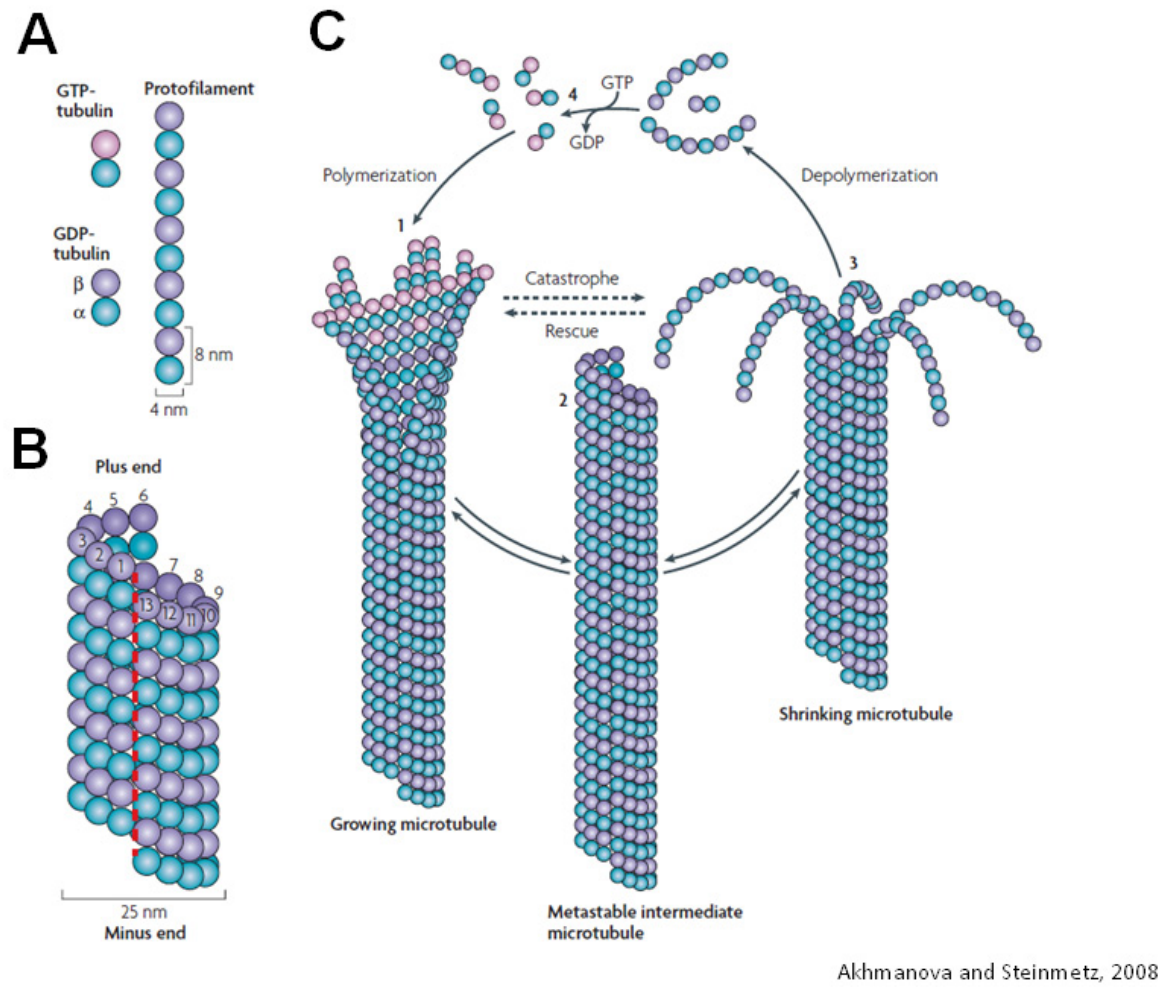

Figure 1. Microtubule structure and dynamic instability.

(A) Tubulin heterodimers are the building blocks for the protofilaments.
(B) Thirteen protofilaments arrange laterally to form a single MT. The MT seam is indicated as a red dotted line.
(C) MT plus ends switch between periods of growth and shrinkage.

Alpha and beta tubulin monomers, having a molecular weight of about 50000 Da each, are ≈50% identical at the amino acid level [8]. However, different isotypes of the monomers are existing. In humans seven alpha and eight beta tubulins are found, whereas budding yeast contains only two α and one β beta tubulin [9]. The folded part, the core, of tubulin isotypes is conserved, whereas their unstructured carboxy terminal tails (CTTs) are more divergent. Beta-tubulin isotypes have the most divergent CTTs and many of these tubulin isotypes

show enrichment in specific cell or tissue types. Adding another level of complexity, the tubulin monomers can be post translationally modified, including polyglutamylation, polyglycylation, detyrosination, acetylation, phosphorylation and palmitoylation. Most of these post-translational modifications occur on the C-terminal tails and the modification enzymes have a strong preference for acting on tubulin subunits already incorporated into MTs [10] [11]. The C-terminus, where the majority of variations among different monomers (different isotypes or through PTMs) of tubulin are located, is exposed on the surface of the MT. That is why variations of monomers are not affecting MT dynamics directly, but rather alter the association between Microtubule associated proteins (MAPs) and the MT lattice.

Although both monomers are able to bind GTP, only the β tubulin can hydrolyse it to GDP [12]. This hydrolysis step is strictly coupled to MT dynamics. While typically dimers with GTP bound polymerize, after polymerization, this nucleotide is hydrolyzed and the resulting GDP becomes nonexchangeable in the context of the microtubule. Protofilaments having GDP bound show a more curved structure than the ones that have GTP bound. This conformational change seems to make the MT more unstable as bent protofilaments are forced to remain straight in the MT assembly [13].

Presumably, growing MTs maintain a so called GTP cap (GTP bound β tubulin at the plus end) necessary for stabilization [14]. Once this GTP cap gets lost, the resulting conformational change might destabilize the lateral attachment of adjacent protofilaments, thereby initiating a catastrophe (rapid depolymerisation) [15]. A shrinking MT is characterized by curling, disintegrating GDP-containing protofilaments at the depolymerising end [16]. Only after depolymerisation GDP bound to tubulin can be again replaced by GTP.

A cell can take advantage of polymerization or depolymerisation of MTs by using these processes to perform mechanical work. For instance in anaphase, shrinking MTs can contribute to chromosome segregation by pulling them to opposing poles. On the other hand, growing MTs can help to push out membranes, or push spindle poles apart during cell division. Therefore, in vivo, microtubule dynamics have to be regulated in a spatiotemporal manner. Such a highly specific regulation of MT dynamics is achieved by so called microtubule-associated proteins (MAPs).

1.2 Microtubule associated proteins

Proteins that interact with MTs, so called MAPs, perform a variety of functions. Some of them influence the stability of MTs, mediate interactions of MTs with other proteins in the cell or crosslink MTs.

Especially during interphase it is often required that MTs are stabilised by so called structural MAPs, like the neuronal proteins MAP2, tau or MAP1A and MAP1B, all four of these being

highly extended and mostly unstructured [17]. Structural MAPs usually consist of repeating domains, allowing them to interact with a couple of MTs simultaneously. They can stiffen MTs [18] [19] and link adjacent protofilaments. In addition, they can also associate with other proteins like actin at the same time, linking the MT and actin cytoskeleton. In vertebrates there is another class of structural MAPs, called STOPs (Stable Tubule Only Polypeptides) that contribute to resistance of MTs to cold [17]. Further known structural MAPs are Lis1 or Doublecortin that play a role in brain development and can stabilize MTs, enhance their polymerization or bundle them. When a cell progresses to M-phase more dynamic MTs are needed and the stabilisation has to be switched off. This can be controlled by kinases and phosphatases [20]. Phosphorylation of MAPs leads in the majority of cases to their detachment from the MTs.

For the cell it is not only important to stabilise MTs, it is also required to destabilise them both spatially and temporally. Proteins like Stathmin, a tubulin-sequestering protein, or Katanin, which can sever MTs into short pieces, fulfil that function. In addition, members of the kinesin family can act as ATP-dependent MT depolymerases. For instance, MCAK, a member of the kinesin-13 family, uses the energy provided by ATP hydrolysis not for moving along MTs but for removing tubulin from the ends of MT [21] . Moreover, some kinesins, that actively move towards a MT end, have an effect on MT dynamics and thereby regulate MT length in cells [22]. Other kinesins, like MKLP1, have additional MT binding sites apart from the motor domain, and, thereby, are able to generate crosslinks between MTs. These kinesins can bundle and slide antiparallel MTs apart, a process needed for spindle elongation during anaphase. However, for some kinesins the only function might be to transport other molecules, e.g. MT regulators, to the ends of MTs.

Among MAPs the γ-TuRCs have a special role. These ~25-nm diameter ring like structures [23] consist of γ-tubulin and specific MAPs and form the microtubule-organizing centres.

Another group of MAPs, essential to assemble certain microtubule-based structures, are MT crosslinking proteins. Among the nonmotor crosslinking proteins, the conserved PRC1/Ase1/MAP65 family has the unique feature to connect pairs of antiparallel MTs [24] (Fig. 2). Recently, the crystal structure for PRC1 was solved displaying that the protein is an elongated rod-shaped molecule [25]. The N-terminus is required for dimerization, while the C-terminal located spectrin domain mediates MT binding (Fig. 2). As the long rod is spacing the two domains, in the homodimer, the two MT interaction domains are separated by 32 nm. This is in agreement with the ~35 nm distance between two crosslinked MTs that was observed in electron microscopy (EM) [26]. Some, like the fission yeast homolog Ase1p even have a function during interphase [27]. It is implicated in forming antiparallel MT bundles along the axis of the rod-shaped cells, with minus ends near the middle of the cell and plus ends facing the cell periphery [28]. This organization of the MT cytoskeleton is required for the linear

growth of fission yeast. Also Map65, the PRC1 plant homolog, bundles MT along the plasma-membrane in interphase, a process involved in axial cell growth [29]. However, most importantly and shared by all members of the PRC1/ Ase1/MAP65 family is the essential role in establishing the central spindle [30] [31] [32].

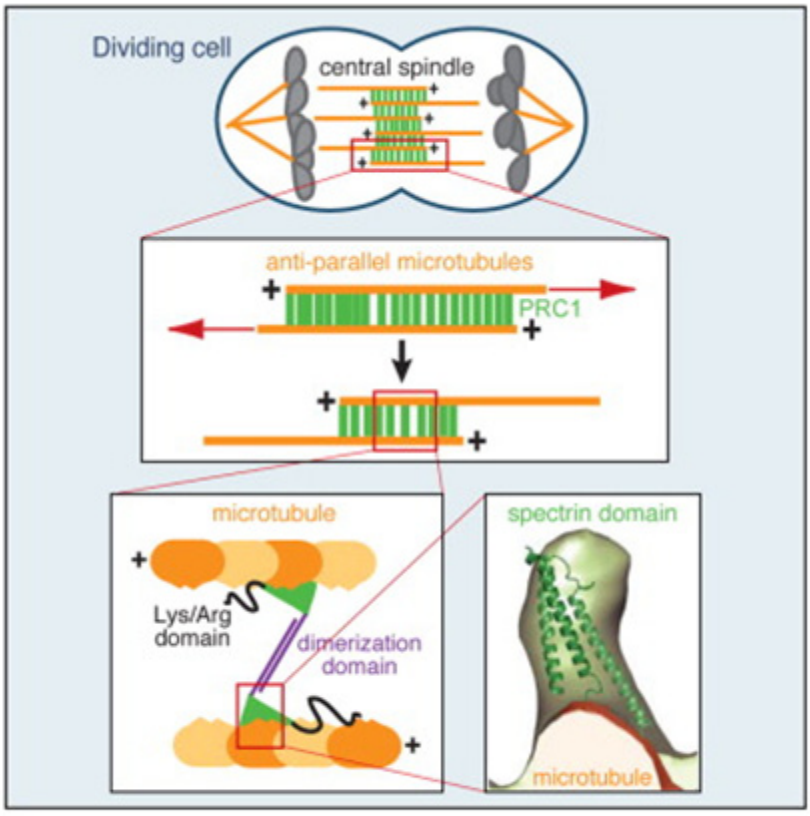

R.Subramanian et al,2010

Figure 2. PRC1 bundles antiparallel microtubules in the spindle midzone.

The other crucial players in setting up a spindle midzone are motor proteins. It is the interplay between them and crosslinking proteins that define the architecture of the central spindle, like spindle length. Interestingly the involved motor proteins differ between species. In budding yeast it is Cin8, a kinesin-5 [33], in fission yeast it is a kinesin-6 [34], while in mammals the interplay between kinesin-4 and PRC1 is required for spindle midzone formation.

Even the mechanism by which the kinesins and the crosslinkers control midzone length is different. Ase1p for instance functions as an adaptive brake, thereby preventing overlapping MTs to slide apart [35]. However that is not the case for PRC1, which is unable to stop complete separation of MTs [26], at least in vitro. In vertebrates, the formation of an antiparallel overlap of fixed length by PRC1 and the kinesin Kif4 seems to depend on the MT growth inhibitory function of Kif4 [36]. It should be mentioned that besides kinesins also nonmotor proteins like CLASPs [37] [38] can be targeted to the spindle midzone by Ase1/PRC1.

In general Ase1/PRC1 function is strictly controlled within cells by different regulatory modes. First the protein levels are under tight control. At least in mammals and budding yeast the amounts stay low except for S and M phase [39] [40]. With mitotic exit the protein is completely degraded in an APC^{cdh1}-dependent manner [41]. Apart from that, the proteins are targets of numerous phosphatases and dephosphatases. Usually Ase1/PRC1 is phosphorylated till anaphase onset, thereby inhibiting an earlier association with kinesins or other binding partners[42].

Another significant group of MAPs are the plus-end tracking proteins (+TIPs) that are localized at the growing MT plus ends, making them perfectly positioned to control MT dynamics, and to serve as link to cellular structures such as cell cortex, kinetochores and endoplasmatic reticulum.

1.3 +TIPs

Plus-end tracking proteins include motor and non motor proteins. In general the different families of +TIPs are structurally unrelated, however, they all accumulate at growing MT plus ends. Human CLIP-170 (Bik1p in budding yeast) was the first protein for which plus end tracking could be shown in vivo [43]. The signal of the green fluorescent protein (GFP) tagged CLIP-170 was observed along the growing plus ends of MTs by live cell imaging. The domains that are required for plus end binding of CLIPs are the cytoskeleton-associated protein glycine-rich (CAP-Gly) domains, of which two are located at the N terminus of the protein. So, each homo-dimer of CLIP-170 has four MT binding domains [44]. The domains consist of a hydrophobic cavity and a conserved GKNDG sequence motif [45]. Another CAP-Gly domain containing protein is p150glued, a component of the dynactin complex that interacts with dynein. Besides two zinc knuckle motifs, CLIPs, unlike p150glued, also possess an EEY/F motif at the very C-terminus. This motif can fold back and interact with one of the proteins own CAP-Gly domains [46]. Initially CLIP-170 was described as a protein that in vitro linked endocytic vesicles to MTs [47]. In addition, the protein is associated with the proper function of kinetochores [48], shows a MT stabilising affect [49] and is required for the localization of dynein, the minus-end-directed MT motor, to MT plus ends [50].

As the name indicates, CLIP-associating proteins (CLASPs), interact with CLIPs and stabilize subsets of MTs under specific conditions [51]. Although CLASP2β was co-pelleting with taxol stabilized MTs [52], it is thought that CLASP proteins are localized to plus ends by associating with CLIPs or EB proteins [53].

Another fascinating class of +TIPs are the XMAP215-like proteins. Mammalian XMAP215 (Microtubule Associated Protein 215 kDa) and Stu2, its budding yeast homolog are able to autonomously localize to MT plus ends in vitro [54]. XMAP215 was first discovered as a factor

that increases MT plus end growth by seven- to tenfold [55]. Consistent with this observation mutants show shorter mitotic spindles in *S. cerevisiae* [56] and aberrations in centrosome integrity, spindle pole organization, and bipolar spindle assembly in Hela cells [57]. XMAP215 proteins are characterized by the conserved N-terminal TOG domains. The number of TOG domains varies between species, with Stu2, a dimer, having two per monomer while monomeric XMAP215 has five. Already a single TOG domain, which is composed of six HEAT-repeat elements that form a paddle-like structures, is sufficient for binding tubulin [58]. XMAP215 binds free tubulin in a 1:1 complex and is thought to stabilize a structural intermediate during the polymerization process. It tracks the plus end during MT growth. Thereby, it is acting as a processive polymerase that stays for numerous rounds of tubulin subunit addition at the plus end. Up to 25 tubulin dimers are added to the growing plus end by a single molecule. Interestingly, in the absence of free tubulin, XMAP215 acts as a MT depolymerase [59].

Although not considered as classical +TIPs motor proteins that can actively walk along MTs powered by ATP hydrolysis, form another group of proteins that can associate with plus ends of MTs. By moving faster than the MT grows, they accumulate at the plus ends [60]. An example is Kip2 (Kinesin-7), which promotes MT stability by targeting Bik1 to the plus end, and is essential for dynein localization at the plus end [49]. Budding yeast Kip3p is also a plus end-directed motor and interestingly a plus end-specific depolymerase [61]. Mammalian MCAK, a potent MT depolymerase, associates also with the tips of growing MTs [62] It is noteworthy that the localization of MCAK at the + end is not due to its intrinsic motor function but depends on other proteins, like EB proteins [63]. The same holds true for the actin based motor protein Myo2, which is necessary for the correct orientation of the pre-anaphase spindle. By binding to Kar9 which interacts with the plus end tracker Bim1, it tracks MT plus ends [64]. Further motor proteins, which are associated with plus ends, are Kar3 and Cik1, which form a heterodimer and are required for karyogamy. The heterodimer depolymerises MTs from the plus ends while keeping the plus-ends attached to the cortex of the schmoo-tip [65].

Most +TIPs are not able to localize to plus ends on their own. Instead they use a common mechanism referred to as „hitchhiking“, meaning that they associate with plus ends via binding other autonomously plus end tracking proteins. Among these autonomously plus end tracking proteins, in the recent years, the End Binding (EB) protein family has emerged as the central player for recruiting other +TIPs to growing MT ends.

1.4 EB proteins

End binding (EB) proteins were first discovered by their ability to bind the Adenomatous polyposis coli (APC) protein, a tumor suppressor, which is often mutated in colorectal cancer

[66]. Later it was shown that EB was responsible for targeting APC to the MT plus end [67]. Initially the ability of EB proteins to localize at MT plus ends was observed in budding yeast [68]. Subsequently this behaviour was also shown in many other systems like mammalian cells [53 69] and in vitro [70].

EB proteins play an important role in all kinds of processes that involve MTs like cell migration, epithelial remodelling, nucleus positioning, vesicle transport [71], cortex attachment of MTs[53] as well as proper assembly, dynamics, and positioning of the mitotic spindle [72]. In addition they are associated with kinetochore function [73]. Humans have three EB paralogs, EB1/2/3, while in budding yeast, EB proteins are represented by a single homolog called Bim1. In general, EB1 and EB3 are considered to have similar functions [74]. There is not much known about the role of EB2, except for being required during apico-basal epithelia cell differentiation [75]. All members of the EB family contain a calponin homology (CH) domain, which mediates binding to MTs, at the N-terminus [76]. It is noteworthy that also another MT binding protein known as NDC80, a kinetochore protein, contains a CH domain. However the MT binding mechanisms for EBs and NDC80 differ [77 78]. For the CH domain of Mal3, the fission yeast homolog of EB1, it was shown that a single domain bridges two adjacent protofilaments by binding at the corner of four tubulin heterodimers. So the binding site consists of two neighbouring α- and β tubulins. Furthermore, the position of the binding site is in close proximity to the GTP hydrolysis site of β tubulin. This allows the CH domain to recognize the GDP/GTP state of the β tubulin, a state that is thought to determine EBs plus end localisation. It seems that EBs preferentially bind to a tubulin conformation that is induced by GTP hydrolysis and exists for several seconds before transforming into the GDP conformation. This would explain the comet like plus end localization of EBs [78]. A flexible linker that can be a target of regulatory phosphorylations [79] connects the N-terminal CH domain with the also conserved C-terminal EBH domain.

The EBH domain, which is required for dimerization, gives rise to a coiled coil structure that folds back on itself. At the end of this structure a short four helix bundle is formed that harbours two hydrophobic cavities [80]. These grooves form the basis for interactions with SxIP (Ser-x-Ile-Pro) sequence motifs containing proteins (Fig. 3) [81]. The EBH domain is surrounded by negatively charged residues, while SxIP sequence motifs are usually embedded in basic and serine rich regions. This leads to the formation of extensive salt bridges that can significantly enhance the interaction between EBs and SxIP sequence motif containing proteins. By comparing the amino acids adjacent to the SxIP sequence of 14 well-known mammalian EB interaction partners, the motif was refined recently. The nine amino acid stretch surrounding the SxIP consensus of (X1-X2-[ST]-X3-[IL]-P-X4-X5-X6) had no acidic amino acids and at least one basic amino acid at one of the positions X1-X4 [82]. Apart from that, the SxIP-containing sequence is generally located in an intrinsically disordered

region and is evolutionarily conserved. It should be noted that of course other variations of this motif (threonine instead of serine and leucine instead of isoleucine) are tolerated and new motifs that bind to the same sites in Bim1 were identified recently (Diss. ETH No. 21563). Phosphorylations close to SxIP sequence motifs can abolish the interaction and add a further level of regulation [83] [84]. SxIP sequence motif containing proteins include numerous functionally diverse proteins like the tumor suppressor APC, the Aurora kinase Ipl1, the regulator of MT dynamics SLAIN2 [85], the MT depolymerase MCAK [81] and many more. The very end of the unstructured C-terminus of EBs terminates in a conserved EEY/F-COO– motif that is very similar to the C-terminus of α tubulin and of CLIP-170 [45].

This is the site, where the second and smaller class of EB-recruited +TIPs binds to (Fig. 3). This class of proteins share a CAP-Gly domain (cytoskeleton-associated glycine-rich) that forms the binding interface. As already mentioned above, it consists of a basic groove, a hydrophobic patch that is also part of the groove and a conserved GKNDG sequence motif [86]. The interaction interface of CAP-Gly domains is not only required for binding to EBs, but is also used to associate with MTs [86]. Interactions are only formed with α tubulin, as its aromatic tyrosine at the end is crucial for binding. Concomitantly, in tubulin tyrosination deficient mutants plus end tracking of CAP-Gly proteins is reduced [87]. The CAP-Gly protein, CLIP-170, is not plus-end tracking autonomously in vitro, but requires both, EB1 and tyrosinated α-tubulin [88]. It should be mentioned, that in budding yeast Bik1p, the CLIP-170 homolog, localizes to plus ends also via active transport by motor proteins [49].

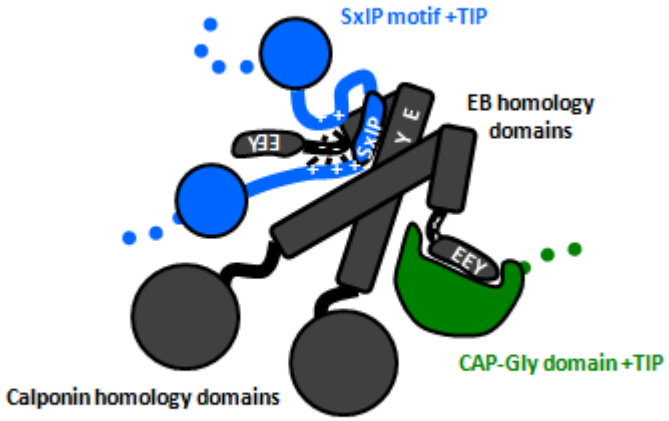

Adapted from T. Wittmann, 2012

Figure 3. EB-dimer and its binding partners.

Besides forming a platform for most known +TIPs, EBs also have direct affects on MTs.
In vitro EB1 accelerates microtubule growth and promotes both catastrophes and rescues [89]. For Mal3 it was also shown that it makes MTs more dynamic [90].

1.5 Bim1

In budding yeast there is only a single EB homolog known as Bim1. *Bim1Δ* strains fail to grow at extreme temperatures ≥37°C or ≤14°C. Cells have short and/or misoriented spindles and are hypersensitive to benomyl. Moreover, defects in karyogamy, nuclear division and alterations in the frequency of binucleate mothers are observed. Apart from that a Bim1 deletion shows synthetic lethality with a large number of proteins including other MAPs like the +TIP, Bik1 [91], MT crosslinker Ase1 [92], nuclear migration factor Num1 [91], spindle checkpoint proteins *bub1-3* [92] as well as a subset of *tub1* conditional-lethal alleles and many more. Interestingly, overexpression of the protein is also lethal. The protein is clearly well conserved over evolutionary time: 33–36% identity and about 56–61% similarity to human, mouse and *S. pombe* [91]. All molecular features required for partner binding and in addition, both, SxIP motif and CAP-Gly domain containing proteins are present in budding yeast.

2. Aims of my project

The complex interplay between all MAPs and their regulators is the key to define the function and structure of MTs. Although in recent years many interactions between MAPs have been characterised, we are still far away from understanding the whole picture. Therefore, it is essential to find out more about how MAPs associate with each other to regulate the MT cytoskeleton.

EB1 proteins serve as the central adaptors of MT tip associated networks on growing MTs by potentially interacting with all other +TIPs. Proteins that associate with EBs can be divided into 2 groups. The first class of proteins contains 1 or more SxIP sequence motifs and binds to the EBH domain of EB1. The second class share a CAP-Gly domain, which associates with the acidic/aromatic C-terminus of EB1.

In addition to functioning as a +TIP platform, EBs can also directly alter MT dynamics in vitro. EB1 proteins belong to a highly conserved protein family and whereas mammals contain three EB paralogs (EB1, EB2 and EB3), in the simple model organism Saccharomyces cerevisiae (budding yeast) EBs are represented by a single homologue called Bim1.

I generated Bim1 mutants that couldn't interact with any or only a subset of +TIPs, but were not altered in their MT binding ability. I aimed to determine the composition of +TIPs associated with these Bim1 versions by performing pull-down assays followed by mass spectrometry.

In addition, I dissected the specific roles of EB1 unable to bind any partners or only a subset of partners on the regulation of the MT cytoskeleton. The Bim1 mutant, losing its function as a central +TIP adaptor, showed similar phenotypes as a bim1 deletion strain.

Apart from that, I identified the PRC1 homologue Ase1, which bundles antiparallel MTs, as a novel binding partner of Bim1 and mapped the interaction interfaces in vivo. In vitro I could show that the interaction is a direct one and that Bim1 can recruit Ase1 to MTs under conditions that do not allow Ase1 alone binding to MTs.

3. Materials and Methods

3.1 Yeast strain construction

Yeast strains were generated using standard protocols. C-terminal tags and deletions were constructed by PCR as described previously [93]. N-terminally tagged Bim1 strains used for mass spectrometry were generated by subcloning the 3´UTR (500 bp), 5´UTR (500 bp), 6xHIS/6xFLAG-tag and the Bim1 ORF into a pRS306 plasmid. C-terminal deletions and EBH-domain mutants were made by using the Phusion Site-Directed Mutagenesis Kit (Thermo Scientific). All C-terminal 6xHIS/6xFLAG tagged Bim1 strains used in this study, as well as the Nup159-HA, Nup159-GFP and their respective SxIP motif mutants were constructed in an analogous manner. Bim1-3xGFP expression vector was generated by subcloning Bim1-3xGFP derived from TZP95 vector into the pRS306-3´UTR-5´UTR plasmid. Vector constructs were integrated, replacing the endogenous WT-locus, by cutting with restriction enzymes between the 3´ and 5´ UTR. If not indicated otherwise, yeast strain experiments were performed in YPD (YP + 2% glucose) or for imaging purposes in minimal medium supplemented with dropout TRP and 2% glucose.

3.2 In vivo FLAG-pull downs from yeast extracts

Asynchronous yeast cultures, that were grown for a couple of hours to reach OD_{600} =1, were harvested at 4°C, washed with H_2O, resuspended in lysis buffer A (25 mM Hepes pH 8.0, 2 mM $MgCl_2$, 0.5 mM EGTA pH 8.0, 0.1 µM EDTA, 0.1% NP-40, 15% glycerol, 150 mM KCl,1x phosphatase inhibitor (0.41mM sodiumpyrophpsphate, 0.25 mM sodium azide, 0,5 mM sodium fluoride, 20 nM sodium orthovanadate), 1x protease inhibitor cocktail set IV (Calbiochem)) and subsequently lysed by bead beating or freezer milling. The cleared lysate was incubated for 1.5 h with α-FLAG M2 antibody (Sigma Aldrich) coupled magnetic Dynabeads (Life Technologies). Samples of the beads, which were washed three times with WB B (25 mM Hepes pH 8.0, 150 mM KCl), were eluted by boiling in SDS sample buffer for 10 min, at 95°C. Analysis was performed by SDS-PAGE and western blotting.

3.3 Mass spectrometry

3.3.1 Sample preparation

In case of using the FLAG-pull down samples for mass spectrometry, the beads, which were incubated for 2 h with the cleared lysate, were washed 3x with buffer A, 4x buffer B, 4x buffer C (25 mM Hepes pH 8.0, 50 mM KCl) and 50 mM TEAB buffer (pH 9). Samples were

digested on beads by incubating with 5 ng/µl LysC, O/N at 37°C. Filtered supernatant was processed by mass spectrometry. Subsequently proteins left on the beads were eluted by 0.1 M glycine (pH 2, adjusted with HCl). Prior to analysing the samples by mass spectrometry, 5% of the samples were loaded on a silver stained gel.

3.3.2 NanoLC-MS Analysis

The nano HPLC system used was an UltiMate 3000 HPLC RSLC nano system (Thermo Fisher Scientific, Amsterdam, Netherlands) coupled to a Q Exactive mass spectrometer (Thermo Fisher Scientific, Bremen, Germany), equipped with a Proxeon nanospray source (Thermo Fisher Scientific, Odense, Denmark). Peptides were loaded onto a trap column (Thermo Fisher Scientific, Amsterdam, Netherlands, PepMap C18, 5 mm × 300 µm ID, 5 µm particles, 100 Å pore size) at a flow rate of 25 µL min^{-1} using 0.1% TFA as mobile phase. After 10 min, the trap column was switched in line with the analytical column (Thermo Fisher Scientific, Amsterdam, Netherlands, PepMap C18, 500 mm × 75 µm ID, 3 µm, 100 Å). Peptides were eluted using a flow rate of 230 nl min^{-1}, and a binary 2h gradient, respectively 165 min.
The gradient starts with the mobile phases: 98% A (water/formic acid, 99.9/0.1, v/v) and 2%B (water/acetonitrile/formic acid, 19.92/80/0.08, v/v/v) increases to 35%B over the next 120 min, followed by a gradient in 5 min to 90%B, stays there for five min and decreases in 5 min back to the gradient 98% A and 2% B for equilibration at 30°C.

The Q Exactive mass spectrometer was operated in data-dependent mode, using a full scan (m/z range 350-1650, nominal resolution of 70,000, target value 1E6) followed by MS/MS scans of the 12 most abundant ions. MS/MS spectra were acquired using normalized collision energy 30%, isolation width of 2 and the target value was set to 5E4. Precursor ions selected for fragmentation (charge state 2 and higher) were put on a dynamic exclusion list for 10 s. Additionally, the underfill ratio was set to 20% resulting in an intensity threshold of 2E4. The peptide match feature and the exclude isotopes feature were enabled.

3.3.3 Data Analysis

For peptide identification, the .RAW-files were loaded into Proteome Discoverer (version 1.4.0.288, Thermo Scientific). All hereby created MS/MS spectra were searched using Mascot 2.2.07 (Matrix Science, London, UK) against the Yeast protein sequence database. The following search parameters were used: Beta-methylthiolation on cysteine was set as a fixed modification, oxidation on methionine, acetylation on lysine and protein-N-terminus and

phosphorylation on serine, threonine and tyrosine were set as variable modifications. Monoisotopic masses were searched within unrestricted protein masses for tryptic peptides. The peptide mass tolerance was set to ±5 ppm and the fragment mass tolerance to ±30 mmu. The maximal number of missed cleavages was set to 2. The result was filtered to 1% FDR using Percolator algorithm integrated in Thermo Proteome Discoverer. The localization of the phosphorylation sites within the peptides was performed with the tool phosphoRS [94].

3.4 Purification of GST-tagged Bim1$^{YE/AA}$ from *E. coli*

GST-tagged Bim1$^{YE/AA}$ was constructed by using the pGEX-TEV-*BIM1*^{WT} plasmid as template and introducing mutations by Phusion Site-Directed Mutagenesis Kit (Thermo Scientific). The derived plasmid was transformed into *E.Coli* BL21 DE3.

Bacteria were always grown in LB containing 100 mg/ml ampicillin. An overnight culture was diluted back to OD_{600} =0.06 and was put at 37°C. After reaching OD_{600} =0.6, protein expression was induced by adding IPTG to a f.c. of 0.1 mM and incubating at 18°C, O/N. The pellet of the harvested cells was resuspended in lysis buffer (1xPBS, 1% triton, 1x protease inhibitor cocktail complete EDTA-free (Roche Diagnostics)). Lysis of cells was achieved by sonication. Cleared lysate was incubated for 2 h with glutathione-sepharose^{TM} 4B (GE Healthcare) and subsequently washed 3x with 0.1% Triton in 1x PBS, further 3x with 0.1% Triton and 500 mM NaCL in 1x PBS and again 3x with 0.1% Triton in 1x PBS. Proteins were kept on the beads for later in vitro binding assays.

3.5 Purification of FLAG-Ase1-HALO from yeast extracts

1xFLAG-Ase1-HALO was cloned into a pESC-TRP vector to generate the expression plasmid JFP15. DDY1810 cells were transformed with this vector and selected on doTrp plates. A 400 ml pre-culture was grown in doTrp medium supplemented with 2 % glucose. The cell suspension was diluted in a final volume of 5 l to OD_{600} =0.06 with doTrp medium supplemented with 2 % raffinose. After reaching an OD_{600} between 1 and 1.4, protein expression was induced by adding galactose to a f.c. of 2 % and YEP to a f.c. of 1x. Before harvesting, cells were kept growing for 16 h at 30°C. The pellet, which was washed with 1x PBS, was resuspended in a minimal amount of PBS to make droplets in liquid nitrogen. Droplets were grinded in a freezer mill. ~20 g freezer mill powder was dissolved in 30 ml buffer A (50 mM Hepes pH 7.4, 250 mM NaCl, 1 mM PMSF, 1% Triton, 0.1 mM EGTA, 0.1 mM EDTA, 1x protease inhibitor cocktail set IV (Calbiochem), 5% Glycerol, 1 mM $MgCl_2$). Lysis occurred on ice and took 30-60 min. Cleared lysate was incubated with 450 µl M2 affinity agarose (Sigma) for 1 h at 4°C. Beads were washed 6x with buffer A containing 150

mM instead of 250 mM NaCl, before eluting with 3x FLAG peptide (2 mg/ml) in 25 mM Hepes and 250 mM KCl. Elutions were supplemented with 5% glycerol.

3.6 Purification of Ase1-STREP variants from SF9 insect cells

Ase1-STREP was cloned into the pFLmut vector. ΔNse1 -STREP was generated by deletion PCR using the Phusion Site-Directed Mutagenesis Kit (Thermo Scientific). For making the bacmid, the pFLmut vectors, harbouring the constructs, were transformed into the DH10Bac *E. coli* strain. White colonies were selected on multibac plates (50 µg/ml Canamycin, 7 µg/ml Gentamycin, 40 µg/ml IPTG, 100 µg/ml X-Galactose, 10 µg/ml Tetracycline) in order to inoculate LB (50 µg/ml Canamycin, 7 µg/ml Gentamycin, 10 µg/ml Tetracycline) for bacmid extraction. After 24 h at 37°C bacmids were purified. Three ml cultures were harvested and resuspended in 300 µl buffer P1 (QIAprep Spin Miniprepr Kit Qiagen). Bacteria were lysed by adding 300 µl buffer P2. Lysis was stopped by the addition of 300 µl N3 buffer after 5 minutes. After centrifugation at 17,900x g for 10 min 700 µl isopropanol were added to the supernatant. DNA was kept at -20°C for 30 minutes to precipitate. After spinning for 1 minute at 17,900x g, the pellet was washed with 70% EtOH and dissolved in H2O. 10x10^6 adherent SF9 (*Spodoptera frugiperda)* cells were transfected by the addition of 300 µl transfection reagent. Transfection reagent contained CellFECTIN^{TM} (Invitrogen) and bacmid DNA, both diluted 1:30 in serum free medium (Sf900 II SFM, Gibco) and mixed at least 20 min before usage. 72 h after transfection the supernatant is used to infect 100 ml of 10x10^6 cells/ml in suspension medium (grace insect cell medium supplemented with 10% FCS (Gibco), 1% PenStrep (Sigma), 20 mM Glutamine (Sigma), 0.1% Pluronic (Gibco)) in order to produce Virus V2. Prior to infecting a 200 ml 0.8x10^6 cells/ml culture, successful protein expression was determined by YFP measurement after 48-72 h. For standard STREP-tag protein purification 200 ml of infected cells were harvested, washed once in PBS and resuspended in 10 ml Lysis buffer (50 mM NaH_2PO_4 pH 8, 300 mM NaCl, 1x protease inhibitor cocktail complete EDTA-free (Roche Diagnostics)). During the purification all steps were done at 4°C. Cell breakage was achieved by using 10x a douncer. Cleared lysate was incubated for 2 h rotating at 4°C with Streptactin Superflow plus (Qiagen). After washing the beads 3x with lysis buffer (without the protease inhibitor) the tagged protein was eluted with elution buffer (50 mM NaH_2PO_4 pH 8, 300 mM NaCl, 2.5 mM Desthiobiotin (Qiagen), 5% Glycerol).

3.7 In vitro binding assays for different Ase1 and Bim1 variants

Glutathione-sepharose™ 4B (GE Healthcare) was washed 3x with WB B (25 mM Hepes pH 8.0, 150 mM KCl) and then incubated with a 0.5 % BSA solution for 30 min. After three further washing steps, the beads were incubated with the different versions of GST-Bim1 and Ase1-STREP in binding buffer (WB B supplemented with 0.05% Tween).
Prior to incubation, Ase1-STREP was already diluted in binding buffer and centrifuged for 10 min at 17,900x g to remove protein aggregates. For the assay only the supernatant was taken.
After 1 h of rotating at 4°C, the beads were washed 5x with WB B and the samples were analysed by SDS-PAGE and Coomassie staining.

3.8 MT cosedimentation assay of Ase1-WT and Ase1ΔN

Tubulin has been isolated as previously described [112]. It should be noted that porcine brain was used instead of bovine brain. Prior to usage, 40 µl aliquots of tubulin (11 mg/ml) were precleared by centrifuging for 5 minutes at 60,000 rpm, 4°C in TLA-100 tubes (Beckmann Instruments). Next, tubulin was supplemented with 2.5 mM GTP and 40 µl G-PEM (50% glycerol in PEM (80 mM Pipes-KOH, 1 mM EGTA, 1 mM $MgCl_2$)) to give a final concentration of 40 µM MTs. After assembling the MTs at 35°C for 30 min, 10 µM taxol was added. MTs were kept at room temperature for at least 10 min. Ase1 protein was diluted in PEM buffer and centrifuged for 5 minutes at 60,000 rpm, rt to get rid of aggregates. For the binding assay 20 µl of Ase1 supernatant and 20 µl of taxol stabilized MTs (at least 6 different dilutions in PEM) were mixed and incubated at rt for 15 minutes. Samples were centrifuged for 20 min, at 60,000 rpm and 25°C. 40 µl of supernatant were supplemented with 20 µl 3x SDS sample buffer, while the pellet was resuspended in 60 µl 1x SDS sample buffer. Equal amounts of volume for the supernatant and the pellet fractions were analysed by SDS-PAGE and Coomassie staining. In case of Ase1-WT the amount of protein in supernatant and pellet was quantified by determining the band intensity of Coomassie-stained SDS-PAGE gels with ImageJ (National Institutes of Health). The resulting data was analysed using prism software (graphpad) (nonlinear regression-binding saturation-one site total fit) to determine the Kd of the Ase1-WT MT complex.

3.9 Live cell imaging

For live cell imaging yeast strains were grown in minimal medium supplemented with doTRP and 2% glucose. During imaging, cells were attached on concanavalin A–coated culture

dishes. Movies and pictures were acquired at 32°C by using Deltavision deconvolution microscopy (Applied Precision, LLC) on an Olympus microscope [IX-71] operated with SoftWoRx (Applied Precision, LLC) . The microscope was equipped with a 100x oil immersion Plan-Apochromat 1.4 NA objective (Olympus) and a CoolSNAP HQ camera (Photometrics). Z stacks were acquired at 1 minute intervals, deconvoluted and projected into two dimensional images (SoftWorx software) and further analyzed by MetaMorph (Molecular Devices).

3.10 TIRF microscopy

3.10.1 Labelling of Ase1 with Alexa 594

Purified protein was incubated with Alexa 594 C5-maleimide on ice in the dark for 2 h. Labelling reaction was stopped by adding 1 mM DTT. Excess of dye was either removed by gel-filtration (see materials and methods, 3.11 SEC) or by using a PD MiniTrap G-25 column (GE Healthcare Life Sciences).
Alternatively Ase1-STREP was labelled, when it was still attached to Streptactin beads. In this case, removal of excess dye was accomplished by washing the beads 6x with purification buffer (50 mM NaH_2PO_4 pH 8, 300 mM NaCl) prior to elution.

3.10.2 Assembling of flow chambers for TIRF microscopy

Silanized glass slides are kept in acetone O/N and subsequently in EtOH for a couple of hours. Flow cells are constructed by placing strips of double stick tape (Scotch 3M) in parallel on a cleaned slide. Prepared coverslips were placed on top to create a chamber with a volume of about 15 µl per channel.
For performing TIRF on taxol stabilised MTs hydrophobic coverslips were used. They were prepared by consecutive sonication in acetone for 15 min and in ethanol for 15 min. Next, coverslips were incubated for 1 h in boiling Piranha solution. After consecutive washing with water, 0.1 M KOH and MilliQ, they were dried with nitrogen. Coverslips were incubated in 5% dichlorodimethylsilane in heptane for 1 h at rt. After washing them with MilliQ, sonicating for 5 min in MilliQ and further sonication for 5 min in chloroform, they were air-dried.
In order to perform TIRF microscopy on dynamic MTs, commercial biotinylated coverslips, were used (BIO_01, Microsurfaces Inc.). Alternatively Biotin-PEG-5K-SVA coated coverslips were prepared as described previously [95].

3.10.3 TIRF microscopy using taxol stabilised MTs

Assembled flow chambers were incubated with αTubulin for 15 min. After washing with PEM buffer, the chambers were incubated with 0.1% w/v pluronic F-127 (Sigma-Aldrich) in PEM for 30 min. Before floating in the taxol stabilised MTs, the chamber was again washed with PEM.

Taxol stabilised MTs were prepared according to the following scheme: 8 µl PEM , 10 µl HiLyte Fluor^{TM} 647 labelled porcine brain Tubulin (Cytoskeleton, Inc.)), 12 µl of 11 mg/ml unlabelled porcine brain Tubulin, 30 µl G-PEM and 0.75 µl of 100 mM GTP were mixed and incubated for 30 min at 35°C. After tubulin assembly, 1.2 µl taxol (0.5 mM in DMSO) was added to stabilize the MTs. Prior to flowing them into the flow chamber, 5µl of the stabilized MTs were diluted in 71.5 µl PEM, 0.5 mg/ml Casein, 0.05% w/v methylcellulose, 5 µM taxol and 1x OS.

Two to five min after taxol stabilised MTs were attached to the coverslip, unbound ones were washed away by floating in 50 µl WB (PEM + 10 µM taxol +1x Oxygen-scavenger mix (4.5 mg/ml glucose, 0.5% β-mercaptoethanol, 0.2 mg/ml glucose-oxidase(Sigma), 35 µg/ml catalase(Sigma) in PEM)). Finally protein samples were floated into the chamber.

Standard flow-in mix contained: 1x OS mix, 16.66 µM Taxol, 0.33 mg/ml of Casein, 0.133% w/v methylcellulose, 66 mM KCl and variable amounts of Bim1 and Ase1 versions.

Images were acquired using a TIRF microscopy system (Carl Zeiss, Inc.) equipped with a 100x α Plan-Apochromat 1.46 NA objective, controlled by Axiovision software (Carl Zeiss, Inc.). Images were taken every 3 seconds using an electron-multiplying charge-coupled device camera (Cascade II, Photometrics).

3.10.4 TIRF microscopy using dynamic MTs

Preparation of biotinylated rhodamine-GMPCPP MTs (“MT-seeds”): 18 µl tubulin (11 mg/ml) + 32 µl PEM buffer were combined to get “unlabeled tubulin”. 20 µl Unlabelled tubulin, 20 µl Biotin tubulin (Cytoskeleton, Inc.), 20 µl HiLyte Fluor^{TM} 647 labelled Tubulin (Cytoskeleton, Inc.) and µl 10 mM GMPCPP were mixed and centrifuged for 15 min at 60,000 rpm, 4°C in TLA-100 tubes (Beckmann Instruments). Aliquots of the SN were stored at -80°C. One µl of the aliquoted MT-seeds, which were thawn and incubated at 37°C for 10 min, were mixed with 5 µl 10x OS, 5 µl Casein (5mg/ml in Brb50), 1.5 µl methylcellulose (2 % w/v) and 37.5 µl PEM to make the final MT-seed mix, used for imaging.

Preparation of dimly labelled tubulin: 10 µl HiLyte Fluor^{TM} 647 labelled Tubulin (Cytoskeleton, Inc.), 10 µl tubulin (11 mg/ml) and 0.5 µl of 100 mM GTP were combined and centrifuged for 5 min at 60,000 rpm, 4°C in TLA-100 tubes (Beckmann Instruments). Aliquots of the SN were

stored at -80°C if not used directly. Five µl of the aliquoted SN were combined with 1.5 µl 10x OS, 1 µl Casein (5 mg/ml in Brb50), 1 µl methylcellulose (2% w/v), 1µl GTP (10 mM) and 5.5 µl PEM.

Assembled flow chambers (see 3.10.2) were incubated with 0.1% w/v pluronic F-127 (Sigma-Aldrich) in PEM for 1 h. After washing with PEM, 15 µl avidin-DN (Vector laboratories) were added to the chamber for 30 minutes. Following another washing step with PEM, 20 µl MT-seed mix were floated in the chamber. After max 5 min unbound MT-seeds were washed away by floating in 50 µl WB (PEM +1x OS mix). Finally the sample proteins were applied to the flow chamber. Standard flow-in mix contained: 5.5 µl dim-tubulin mix, 1.5 µl 10x OS, 1 µl methylcellulose (2% w/v), 1 µl Casein (5 mg/ml in Brb50), various amounts of sample proteins and PEM buffer for reaching a final volume of 15 µl. Moreover, the salt concentration was always adjusted to 175 mM by adding KCl. For Image acquisition see 3.10.3.

3.11 Size exclusion chromatography (SEC)

SEC was performed on an Ettan LC using a Superose 6 PC 3.2/30 (GE Healthcare Life Sciences) column. As standard gel filtration buffer the Ase1 STREP purification buffer (50 mM NaH_2PO_4 pH 8, 300 mM NaCl) was used. Prior to loading the sample proteins, which were diluted in gel filtration buffer, onto the column, the column was pre-equilibrated with degased H_2O and subsequently degased gel filtration buffer. All run parameters such as flow rate were kept constant during the different runs in order to compare the elution profiles of different protein mixtures.

Table 1: DNA constructs used in this study

Plasmid number	Description
TZP12	pGEX TEV-*BIM1*^{WT}
TZP95	pRS305 XhoI-*Bim1*^{WT} -BamHi-3GFP-XbaI
JFP1	pGEX TEV-*BIM1*$^{YE/AA}$
JFP2	pRS306 NotI-3´UTR-EcoRI-5´UTR-HindIII-*BIM1*^{WT}-3xGFP-SalI
JFP3	pRS306 NotI-3´UTR-EcoRI-5´UTR-HindIII-*BIM1*$^{YE/AA}$-3xGFP-SalI
JFP4	pRS306 NotI-3´UTR-EcoRI-5´UTR-HindIII-6xHis/6xFLAG- HindIII-*BIM1*^{WT}
JFP5	pRS306 NotI-3´UTR-EcoRI-5´UTR-HindIII-6xHis/6xFLAG- HindIII-*BIM1*$^{\Delta CT}$
JFP6	pRS306 NotI-3´UTR-EcoRI-5´UTR-HindIII-6xHis/6xFLAG- HindIII-*BIM1*$^{YE/AA}$
JFP7	pRS306 NotI-3´UTR-EcoRI-5´UTR-HindIII-6xHis/6xFLAG-HindIII-Bim1$^{YE/AA\ ,\Delta CT}$
JFP8	pRS306 NotI-3´UTR-EcoRI-5´UTR-*BIM1*^{WT}-6xHis/6xFLAG-HindIII
JFP9	pRS306 NotI-3´UTR-EcoRI-5´UTR-*BIM*$^{YE/AA}$-6xHis/6xFLAG-HindIII

JFP10	pRS304 NotI-3´UTR-EcoRI-5´UTR-*BIM1*^{WT}-6xHis/6xFLAG-HindIII
JFP11	pRS304 NotI-3´UTR-EcoRI-5´UTR-*BIM1*$^{YE/AA}$-6xHis/6xFLAG-HindIII
JFP12	pRS306 SacI-3´UTR-NotI-5´UTR-*Nup159*^{WT}-XmaI-HA-EcoRI
JFP13	pRS306 SacI-3´UTR-NotI-5´UTR-*Nup159*$^{SXNN1/2}$-XmaI-HA-EcoRI
JFP13	pRS306 SacI-3´UTR-NotI-5´UTR-*Nup159*^{WT}-XmaI-1xGFP-EcoRI
JFP14	pRS306 SacI-3´UTR-NotI-5´UTR-*Nup159*$^{SXNN1/2}$-XmaI-1xGFP-EcoRI
JFP15	pESC^{TRP} NotI-1xFLAG-Ase1^{WT}-SpeI-HALO-SacI
JFP16	pFLmut BamHI-Ase1^{WT}-STREP-SacI
JFP17	pFLmut BamHI-Ase1$^{\Delta N}$-STREP-SacI
BVP1	pRS306 SacI-3'UTR-NotI-5'UTR-AseI-SpeI-3xHA-XmaI
BVP2	pRS306 SacI-3'UTR-NotI-5'UTR-AseI-SpeI-1xGFP-XmaI

Table 2: Yeast strains used in this study

Strain number	Genotype
DDY1810	Mat a, leu2, trp1, ura3-52, prb1-1122, pep4-3, pre1-451
DDY904	Mat α, lys2-801am, leu2-3,112, his3Δ200, ura3-52
DDY1503	Mat a, his3Δ200, leu2-3,112, ura3-52, ade2-101,mad1::URA3
BVY6	Mat a, leu2, trp1, ura3-52, prb1-1122, pep4-3, pre1-451, Bim1^{WT}-6xHIS6xFLAG::KanMx
BVY61	Mat α, lys2-801am, leu2-3,112, his3Δ200, ura3-52, Bim1Δ:URA
BVY98	Mat a, leu2, trp1, ura3-52, prb1-1122, pep4-3, pre1-451, 6xHIS6xFLAG-Bim1^{WT}::URA
BVY99	Mat a, leu2, trp1, ura3-52, prb1-1122, pep4-3, pre1-451, 6xHIS6xFLAG-Bim1$^{\Delta CT}$ -::URA
BVY100	Mat a, leu2, trp1, ura3-52, prb1-1122, pep4-3, pre1-451, 6xHIS6xFLAG-Bim1$^{YE/AA}$::URA
BVY101	Mat a, leu2, trp1, ura3-52, prb1-1122, pep4-3, pre1-451, 6xHIS6xFLAG-*BIM1*$^{\Delta CT, YE/AA}$::URA
BVY214	Mat a, leu2, trp1, ura3-52, prb1-1122, pep4-3, pre1-451, Bim1^{WT}-6xHIS6xFLAG::TRP, HA-Kog1::URA
BVY215	Mat a, leu2, trp1, ura3-52, prb1-1122, pep4-3, pre1-451, Bim1$^{YE/AA}$-6xHIS6xFLAG::TRP, HA-Kog1::URA
BVY208	Mat a, leu2, trp1, ura3-52, prb1-1122, pep4-3, pre1-451, Bim1^{WT}-6xHIS6xFLAG::URA, Bck1-HA::KanMx
BVY209	Mat a, leu2, trp1, ura3-52, prb1-1122, pep4-3, pre1-451, Bim1$^{YE/AA}$-6xHIS6xFLAG::URA, Bck1-HA::KanMx
BVY137	Mat a, leu2, trp1, ura3-52, prb1-1122, pep4-3, pre1-451, Bim1^{WT}-

	6xHIS6xFLAG::KanMx, NUP159^{WT}-3xHA::URA
BVY139	Mat a, leu2, trp1, ura3-52, prb1-1122, pep4-3, pre1-451, Bim1^{WT}-6xHIS6xFLAG::KanMx, NUP159-3xHA$^{SXNN1/2}$::URA
BVY140	Mat α, lys2-801am, leu2-3,112, his3Δ200, ura3-52, NUP159-GFP ^{WT}::URA, spc42-mCherry::KanMx
BVY141	Mat α, lys2-801am, leu2-3,112, his3Δ200, ura3-52, NUP159-GFP $^{SXNN1/2}$::URA, spc42-mCherry::KanMx
BVY151	Mat α, lys2-801am, leu2-3,112, his3Δ200, ura3-52, NUP159-GFP ^{WT}::URA, Bim1^{WT}-mCherry::KanMx
BVY152	Mat α, lys2-801am, leu2-3,112, his3Δ200, ura3-52, NUP159-GFP $^{SXNN1/2}$::URA, Bim1^{WT}-mCherry::KanMx
BVY161	Mat a, leu2, trp1, ura3-52, prb1-1122, pep4-3, pre1-451, Bim1^{WT}-6xHIS6xFLAG::TRP, NUP159 ^{WT}3x-HA::URA
BVY162	Mat a, leu2, trp1, ura3-52, prb1-1122, pep4-3, pre1-451, Bim1$^{YE/AA}$-6xHIS6xFLAG::TRP, NUP159 ^{WT}-3xHA::URA
BVY218	Mat α, lys2-801am, leu2-3,112, his3Δ200, ura3-52, Bim1^{WT}-3xGFP::URA, Spc42-mCherry::KanMx
BVY237	Mat α, lys2-801am, leu2-3,112, his3Δ200, ura3-52, Bim1$^{YE/AA}$-3xGFP::URA, Spc42-mCherry::KanMx
BVY185	Mat a, leu2, trp1, ura3-52, prb1-1122, pep4-3, pre1-451, Bim1^{WT}-6xHIS6xFLAG::URA
BVY186	Mat a, leu2, trp1, ura3-52, prb1-1122, pep4-3, pre1-451, Bim1$^{YE/AA}$-6xHIS6xFLAG::URA
BVY106	Mat a, leu2, trp1, ura3-52, prb1-1122, pep4-3, pre1-451, Bim1^{WT}-6xHIS6xFLAG::KanMx, Ase1-3xHA ^{WT}::URA
BVY107	Mat a, leu2, trp1, ura3-52, prb1-1122, pep4-3, pre1-451, Bim1^{WT}-6xHIS6xFLAG::KanMx, Ase1-3xHA$^{SXNN1/2}$::URA
BVY212	Mat a, leu2, trp1, ura3-52, prb1-1122, pep4-3, pre1-451, Bim1^{WT}-6xHIS6xFLAG::TRP, Ase1-3xHA ^{WT}::URA
BVY213	Mat a, leu2, trp1, ura3-52, prb1-1122, pep4-3, pre1-451, Bim1$^{YE/AA}$-6xHIS6xFLAG::TRP, Ase1-3xHA ^{WT}::URA
BVY222	Mat α, lys2-801am, leu2-3,112, his3Δ200, ura3-52, Bim1^{WT}-3xGFP::URA, Ase1Δ::LEU, Spc42-mCherry::KanMx
BVY223	Mat a, leu2, trp1, ura3-52, prb1-1122, pep4-3, pre1-451, Bim1^{WT}-6xHIS6xFLAG::TRP, Ase1$^{\Delta N}$-3xHA::URA
BVY239	Mat a, leu2, trp1, ura3-52, prb1-1122, pep4-3, pre1-451, Bim1^{WT}-mCherry::KanMx , Ase1$^{\Delta N}$-GFP::URA

4. Results

4.1 Identification and characterization of EB1 interaction partners using different EB1 mutants in budding yeast

4.1.1 Description of the N-terminally tagged Bim1 binding mutants

Initially my aim was to determine the composition of +TIPs associated with Bim1 mutants, unable to bind any or only a subset of MAPs. For abrogating interactions with SxIP (serine – any amino acid – isoleucine – proline) motif containing proteins I generated an Y220/A, E228/A double mutant. Y220 and E228 are two highly conserved amino acids and part of the EBH domain (Fig. 4C), which mediates binding to SxIP motifs. The substitution of these two amino acids by alanines leads to the disruption of hydrogen bond formation (Fig. 4A). It was shown that these mutations are sufficient to disturb the interaction of EB3 with the SxIP sequence motif containing MT depolymerising kinesin, MCAK [96]. In order to diminish the interaction of Bim1 with CAP-Gly domain containing proteins the last four amino acids, which contain conserved acidic amino acids and an aromatic residue, were deleted (Fig. 4B/D). I chose to tag the mutants N-terminally, because tagging Bim1 at the C-terminus is already sufficient to disturb the interaction with CAP-Gly domain containing proteins. For instance, CLIP-170 disappears from the MT +ends in cells expressing EB1-GFP [97]. So, by tagging C-terminally I wouldn´t have been able to pull proteins that only bind via the C-terminus, but not via the EBH domain of Bim1.

To determine the binding partners of the Bim1 variants by performing pull-down assays followed by mass spectrometry or western blot analysis I chose to use a 6xHis6xFLAG tag.

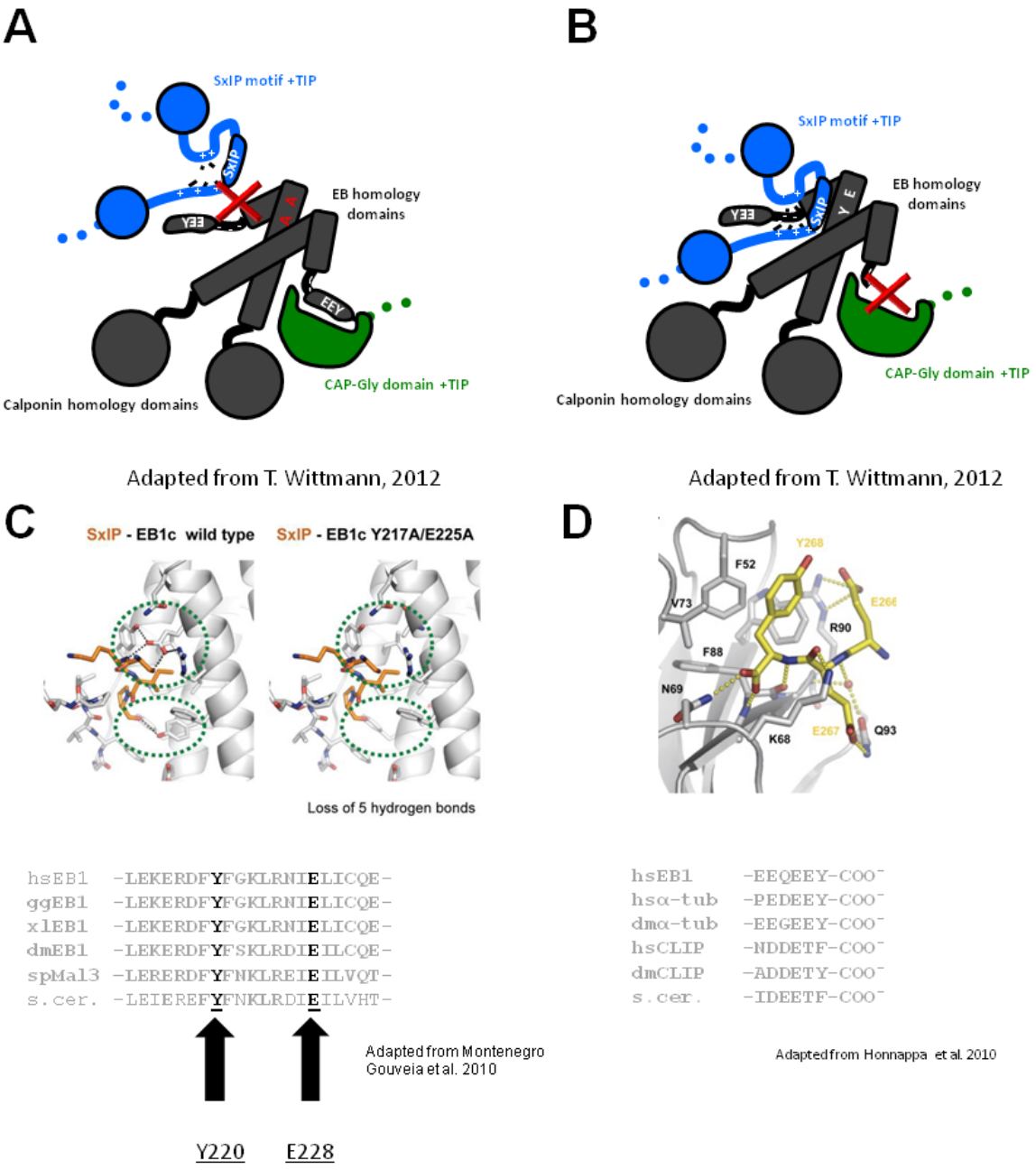

Figure 4 Characteristics of the Bim1 binding mutants.

(A) Schematic shows that Bim1YE/AA does not interact with SxIP motif containing proteins anymore.
(B) Schematic shows that Bim1ΔCT does not interact with CAP-Gly proteins anymore.
(C) Crystal structure of EB1 binding to a SxIP peptide of the kinesin MACF. Replacing the conserved tyrosine 217 and glutamic acid 225 in the conserved EBH domain results in a loss of 5 hydrogen bonds with SxIP peptides. Sequence alignments show the conservation of the EBH domain in EB1 from different organisms. Y220 and E228 are marked black.
(D) Crystal structure of the carboxy-terminal domain of EB1 and the N-terminal CAP-Gly domain of the dynactin large subunit p150glued. Sequence alignments show the conservation between the C-termini of EB1, α-tub, CLIP-170, and Bim1.

4.1.2 Testing cargo interactions of mutant Bim1 variants

The mutant constructs were integrated at the endogenous Bim1 locus, thereby replacing the wild type copy. To see if the mutant strains show the predicted deficiencies in binding to partner proteins I used flag-pull downs followed by western blot. The FLAG-Bim1$^{\Delta CT}$ mutant is indeed unable to interact with Bik1 in vivo. Bik1, the CLIP-170 homolog, is a known CAP-Gly domain containing binding partner of Bim1 [98]. This indicates that the deletion is sufficient to abrogate binding to proteins via the CAP-GLY domain (Fig. 5A). For testing the Bim1$^{YE/AA}$ mutant, my aim was to use Ipl1 as a representative SxIP motif containing binding partner. For Ipl1 it was shown that it binds to Bim1 via two SxIP sequence motifs and mutations in these motifs abolished the interaction in vitro [84]. However, a FLAG-Bim1$^{YE/AA}$/Ipl1-3xHA strain was inviable. Therefore I used Kog1 as an exemplary protein. Kog1, which is part of the TOR complex 1 associates also with Bim1 via two SxIP sequence motifs (Van der Vaart, personal communication). Indeed the introduced mutations in the EBH domain are sufficient to greatly diminish the binding of Kog1 to Bim1, in vivo (Fig. 5B).

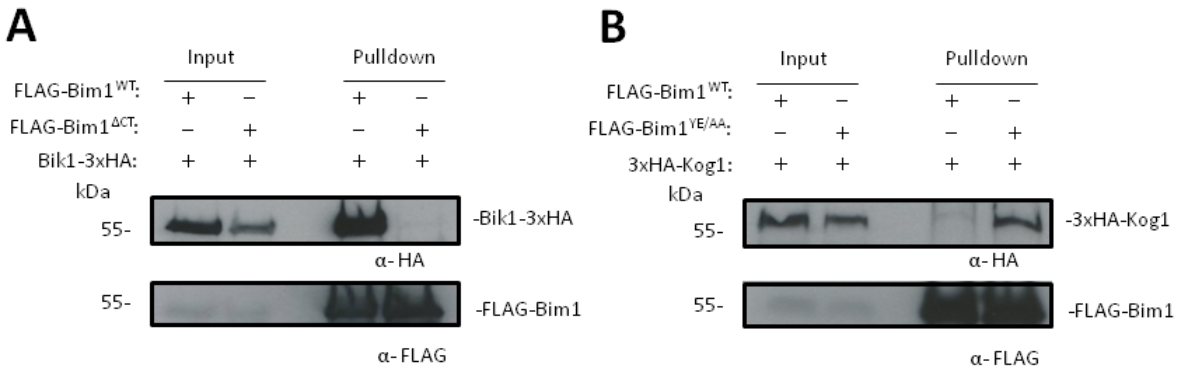

Figure 5. Verification of the Bim1 mutants by pulling down known interaction partners.

(A) Testing the ability of FLAG-Bim1$^{\Delta CT}$ to pull down Bik1 in vivo.
(B) Testing the ability of FLAG-Bim1$^{YE/AA}$ to pull down Kog1 in vivo.

4.1.3 Identification of proteins that associate with the N-terminally tagged binding mutants of Bim1

After verifying that the introduced mutations affect partner binding of Bim1, I wanted to analyse the complete +TIP composition that associates with these mutants. To this end, pull downs using α-FLAG coupled magnetic beads were analysed by mass spectrometry. In Bim1 wild-type controls Kar9 was the major interaction partner (Fig 6 A/B). Kar9, the adenomatous polyposis coli (APC) homolog, mediates the cortical attachment of cytoplasmic MTs and is required for correct positioning of the mitotic spindle [99] [100]. It was no surprise that

Kar9 topped the list, as it is an important known binding partner. This showed that the pull-down and purification procedure itself worked. Kar9 was not pulled down by the YE/AA mutant strains. This was expected, as Kar9 interacts with Bim1 via one SxIP motif and a newly discovered linear motif Leu-x-x-Pro-Thr-Pro-Leu (LxxPTPL) (Diss. ETH No. 21563). As already shown in the analysis of pull down samples by western blot Bik1 is only pulled down with FLAG-Bim1^{WT} and FLAG-Bim1$^{YE/AA}$ but not with the strains lacking the C-terminal part. It should be noted that in the sample of Bim1 ^{WT}-FLAG no Bik1 peptides are detected. This is consistent with the fact that tags at the C-terminus of Bim1 interfere with binding to CAP-Gly domains[97].

The identification of Kog1 in the WT samples but not in the Bim1$^{YE/AA}$ mutants is in agreement with the results from the western blot analysis. I would expect to pull down Kog1 also in the FLAG-Bim1$^{\Delta CT}$ strain, however even in the FLAG-Bim1^{WT} samples only 3 Kog1 peptides were identified. Moreover, the amount of FLAG-Bim1^{WT} compared to FLAG-Bim1$^{\Delta CT}$ was significantly higher. Therefore I cannot draw a conclusion about the ability of Bim1$^{\Delta CT}$ to bind Kog1, based on this experiment. However, this could be easily tested by pull-downs followed by western blot.

As expected, none of the known interaction partners of Bim1 are pulled down by the Bim1$^{YE/AA\ \Delta CT}$, which should have completely lost its function as an adaptor protein for other +TIPs. Interestingly, for some proteins that are involved in the same pathways as Bim1, like Num1, the dynein partner required for nuclear migration, the peptide counts are even higher than in the WT sample. A possible explanation for that observation could be that the double mutant is not able to interact with its “normal” interaction partners anymore and thereby can more easily associate with other proteins.

It is noteworthy that in general the peptide counts for the N-terminally tagged samples were much lower than the C-terminally tagged comparison sample. This was even the case for the bait protein that is why I checked the protein levels of Bim1 in the used strains. Indeed the protein level of Bim1-FLAG in cells was about three fold higher than any of the N-terminally tagged versions (Fig. 6C). The levels between the N-terminally tagged versions showed no detectable difference. This clearly indicated that the position of the tag caused the alteration of protein levels.

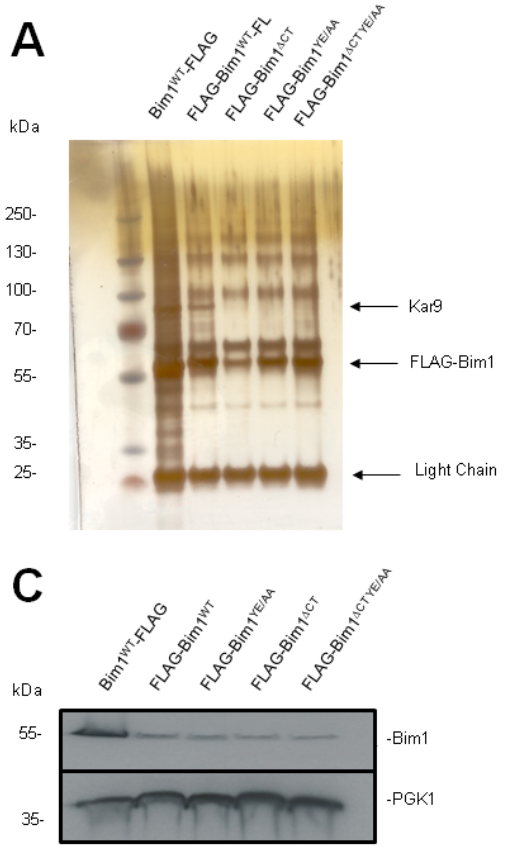

B

Name	Function	Bim1-FLAG (Babet)	N-terminal tagged FL	ΔCT	YE/AA	ΔCT YE/AA
Bim1		30	18 14	8 14	15 14	14 15
KAR9	Bim1 binding protein required for spindle positioning	46	32 **28**	3 **23**	0 **1**	0 **0**
Stu2	Bim1 binding partner, microtubule polymerase	4	0 **1**	0 **0**	0 **0**	0 **0**
Fin1	Spindle pole body-related intermediate filament protein	15	1 5	5 4	6 7	1 8
Num1	Dynein partner required for nuclear migration	10	0 0	0 0	0 0	5 0
Tco89	Target of rapamycin complex 1 component	36	4 0	0 0	0 0	1 0
Kog1	Target of rapamycin complex 1 component	23	**3** 0	**0** 0	**0** 0	**0** 0
Stm1	Involved in Tor signaling, translation under nutrient stress	17	6 4	5 4	8 3	13 4
Gin4	Protein kinase involved in bud growth and septin ring assembly	8	0 0	0 0	0 0	10 0
Pgk1	3-phosphoglycerate kinase involved in glycolysis	4	23 4	20 8	23 7	29 10
Bck1	MAPKKK acting in the protein kinase C signaling pathway	12	7 0	0 0	0 0	13 0
Pma1	Plasma membrane H+-ATPase drives secondary nutrient import	14	9 12	7 16	10 12	16 9
BMH1	14-3-3 protein involved in e.g. rapamycin-sensitive signaling	7	4 2	1 0	3 0	6 1
CCT8	required for the assembly of actin and tubulins in vivo		7 5	0 0	1 2	5 1
Bik1/Clip 170	Microtubule-associated protein		0 **3**	0 **0**	0 **3**	0 **0**

Figure 6. Interaction partners of different N-terminally tagged Bim1 variants.

(A) Silver stained gel displaying pull down samples of different Bim1 variants.
(B) Table of selected peptide scores from the mass spectrometry analysis of pull downs, using different Bim1 variants. Peptide scores labelled in red, indicate known interaction partners.
(C) Comparison of protein levels between the C-terminally and N-terminally tagged Bim1 strains.Pgk1 was used as a reference protein.

4.1.4 Determining the phenotype of N-terminally tagged Bim1 cargo binding mutants

Bim1 serves as the central hub of MT tip associated networks on growing MTs by potentially interacting with all other +TIPs. Interfering with its ability to bind other proteins should have an impact on the MT cytoskeleton and thereby also influence the viability of strains carrying binding mutants.

Spot assays indicated, that the FLAG-Bim1$^{YE/AA}$ mutant strain shows increased sensitivity to benomyl and rapamycin compared to FLAG-Bim1^{WT} (Fig. 7) (data only shown for 25°C, temperatures tested: 25°C, 30°C, 34°C, 37°C). The loss of Bim1´s ability to interact with proteins via its EBH domain correlates with a perturbation of the MT cytoskeleton. In line with this, the MT destabilizing drug benomyl enhances this phenotype. The sensitivity to rapamycin treatment could indicate that Bim1 plays a role in the Tor signaling pathway.

However it could also reflect an independent effect and rapamycin treatment could be an additional stress factor for the cells.

The Bim1$^{\Delta CT}$ strain, which correlates with a loss of binding to CAP-Gly domain containing proteins, like Bik1, performs slightly better than a Bim1$^{YE/AA}$ mutant strain. Apart from that, the double mutant did not seem to be less viable than the Bim1$^{YE/AA}$ mutant strain.

These results indicate that it is more important for the cell to recruit the SxIP motif containing proteins to the MT plus end, than proteins with CAP-Gly domains. This could be explained by the fact that the majority of Bim1 binding partners associate with the protein via the EBH domain and not via the C-terminus.

Another interesting observation is that FLAG-Bim1^{WT} and Bim1^{WT}-Flag behave similarly (Fig. 7). However, it is quite difficult to compare Bim1^{WT}-FLAG and FLAG-Bim1^{WT}. The N-terminally tagged protein is about three times less abundant in cells and probably part of it even mislocalizes, because of its altered ability to bind MTs. On the other hand, the C-terminally tagged version loses its ability to interact with another +TIP protein, Bik1.

In this assay the Bim1Δ strain performed better than the tagged Bim1 strains and at least as well as the DDY1810 control strain. This could be due to the fact that the Bim1 deletion was integrated in the DDY904 background strain (see materials and methods). As DDY1810, which also served as the background strain of the tagged Bim1 strain, harbors additional mutations (see materials and methods) no real comparison is possible. It should be noted that the Bim1 deletion in DDY904 background was even viable at 37°C, which is contradictory to the literature [91], but can be explained by the differences in background.

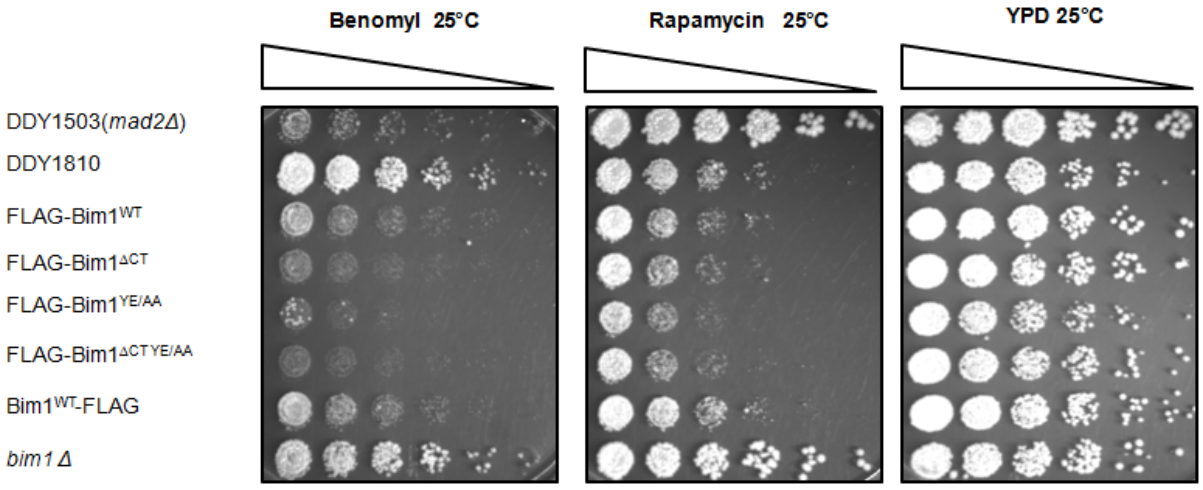

Figure 7. Effects of Bim1 cargo binding mutants on cell viability.

FLAG-Bim1 variants were tested for sensitivity to the MT destabilizing drug benomyl or the inhibitor of Tor –signalling rapamycin. 10 µg/ml benomyl, and 3 nM rapamycin were used, serial dilutions (1:4) of equal numbers of cells were spotted onto the indicated plates. DDY1503 served as a positive control for benomyl sensitivity; DDY1810, the background strain, was used as a reference strain.

4.1.5 Identification of proteins that associate with the C-terminally tagged binding mutants of Bim1

Tagging Bim1 at the N-terminus reduces its protein levels by about three fold (Fig. 6C). This obviously results in low peptide counts of the mass spectrometry analysis compared to Bim1-FLAG, when using the same amount of input material. Therefore low abundant binding partners could be missed in my experiments. I first tried to increase the amount of yeast extract used for the purification (increasing the culture volume from 2 to 5 l), but this did not lead to a significant improvement of peptide scores.

The N-terminal tag might not only affect Bim1 protein levels, it additionally might lead to a mislocalization of Bim1 due to an altered ability to bind MTs [97]. If this was the case, I might even pull down proteins that usually would not interact with Bim1, because they would be simply localized elsewhere in the cell.

Therefore we decided to switch to using C-terminally tagged mutants. As tagging the protein at the C-terminus already abolishes interaction with one class of binding partners, I was limited to the comparison of Bim1^{WT}- and Bim1$^{YE/AA}$-FLAG, a mutant that should completely lose its function as an adaptor (Fig. 8)

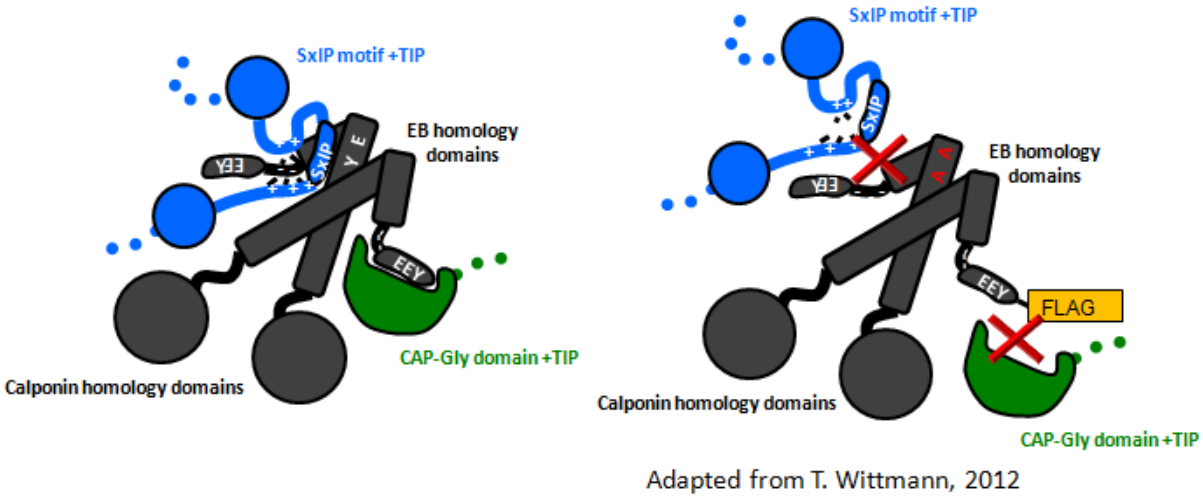

Figure 8. Model of Bim1^{WT} binding to its interaction partners and the cargo deficient Bim1$^{YE/AA}$ mutant.

Replacing a conserved tyrosine and glutamic acid by two alanines in the EBH domain abolishes binding to SxIP motif containing +TIPs. Additionally the FLAG tag at the C-terminus inhibits the association with CAP-Gly domains.

My aim was to identify new Bim1 interaction partners that bind via the known interaction motifs. Therefore, I again performed pull downs followed by mass spectrometry to ideally get the complete set of interaction partners. The comparison between the WT and the cargo deficient mutant would allow me then to discriminate between proteins that bind via the known interaction domains and proteins that either associate with Bim1 unspecifically or via unknown mechanisms. The constructs were again integrated at the endogenous Bim1 locus, thereby replacing the wild type copy.

Before performing mass spectrometry, I tested the mutant by in vivo pull-downs followed by western blot. Although the level of mutated Bim1 in the cell was significantly higher this time compared to FLAG-Bim1, Kog1, as expected, still did not interact with the Bim1$^{YE/AA}$-FLAG mutant (Fig. 9).

The analysis of the peptide scores, gained from the mass spectrometry analysis, also revealed the loss of interaction with Kog1 in the Bim1$^{YE/AA}$-FLAG mutant strain (Fig. 10A/B). Additionally, most of the other proteins belonging to the Tor signaling pathway were not among the hits anymore. The same was the case for all components of the kinetochore and the chromosomal passenger complex. Most importantly the known interaction partners like Kar9, Ipl1 [79], Stu2 [101], or Cik1 (Mieck, personal communication) were not among the hits anymore, indicating that the mutant indeed abolishes interaction via SxIP motifs. As expected in the Bim1^{WT}-FLAG as well as the Bim1$^{YE/AA}$-FLAG sample the CAP-Gly domain containing protein, Bik1, was not pulled down. I therefore conclude that this mutant is indeed unable to bind other +TIPs, thereby losing its ability to target other proteins to the growing MT plus ends. I will refer to the mutant from now on as the cargo deficient mutant.

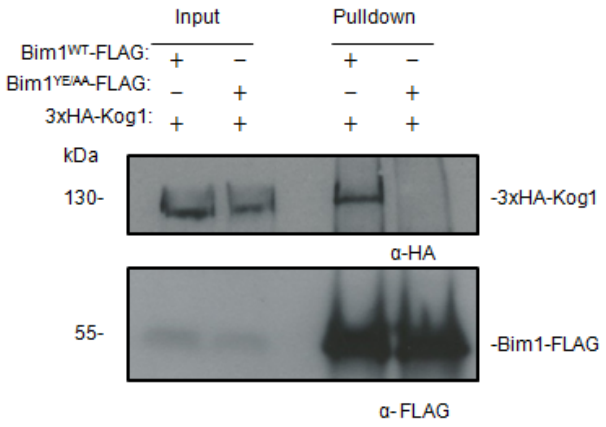

Figure 9. Verification of the Bim1$^{YE/AA}$-FLAG mutant by pulling down a known interaction partner.

Testing the ability of Bim1$^{YE/AA}$-FLAG to pull down the SxIP motif containing protein, Kog1, in vivo.

A

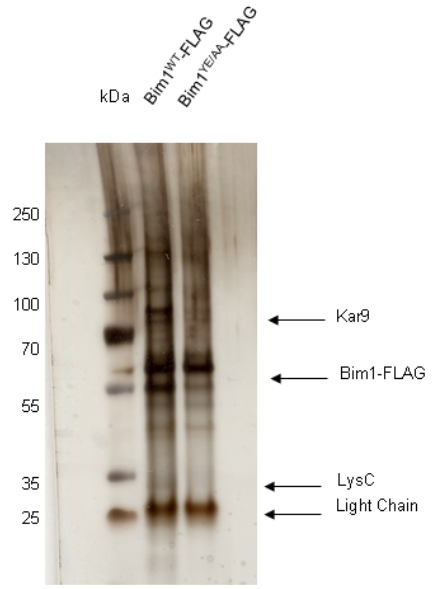

B

	Unique peptide counts	
Name	WT	YE/AA
Bim1	**26**	**18**
Kar9/APC-like	**33**	**0**
Stu2/XMAP215	**3**	**0**
Bir1/Survivin	27	0
Ipl1/Aurora kinase	**6**	**0**
Sli15/INCENP	24	0
Ase1/PRC1	**11**	**0**
Fin1	16	8
Num1	0	3
Cik1	**19**	**0**
Kar3	20	0
She1	4	0
Tco89	33	0
Ksp1	14	0
Kog1/Raptor	**37**	**0**
Tor1	61	0
Lst8	10	0
Stm1	10	9
Spc105	2	0
Tid3/Ndc80	7	0
Nuf2	2	0
Dsn1	2	0
Dam1	2	0

Chromosomal passenger complex

MAPs

TOR1 signalling

Kinetochore

Figure 10. Comparing the interaction partners of Bim1^{WT} and the "cargo deficient" mutant.

(A) Silver stained gel displaying pull down samples of Bim1^{WT}-FLAG and Bim1$^{YE/AA}$-FLAG.
(B) Table of selected peptide scores from the mass spectrometry analysis of pull downs using Bim1^{WT}-FLAG and Bim1$^{YE/AA}$-FLAG strains. Peptide scores labelled in red indicate known interaction partners.

4.2 A Bim1 mutant, unable to bind to interaction partners, shows similar phenotypes as a Bim1 deletion strain

I reasoned that in the cargo deficient mutant strain the majority of MAPs are removed from MT plus ends, because Bim1 does not recruit them anymore. This should perturb the MT cytoskeleton and lead to a growth defect or decreased viability. I aimed to address this by performing spot assays and live cell imaging.

4.2.1 Growth defect analysis by spot assays

Spotting assays indicated that the cargo deficient mutant shows no phenotype on YPD at any of the tested temperatures (Fig. 11) (data only shown for 25°C, temperatures tested: 25°C, 30°C, 34°C, 37°C). But the mutant is clearly sensitive to the MT destabilizing drug

benomyl, however only at 25°C. Interestingly, the cargo deficient mutant does not perform better than a Bim1 deletion strain. Bim1^{WT}-3xGFP shows in comparison to the background strain sensitivity to high amounts of benoyml. This was not surprising, as C-terminally tagged Bim1 WT cannot target Bik1 to MT plus ends anymore.

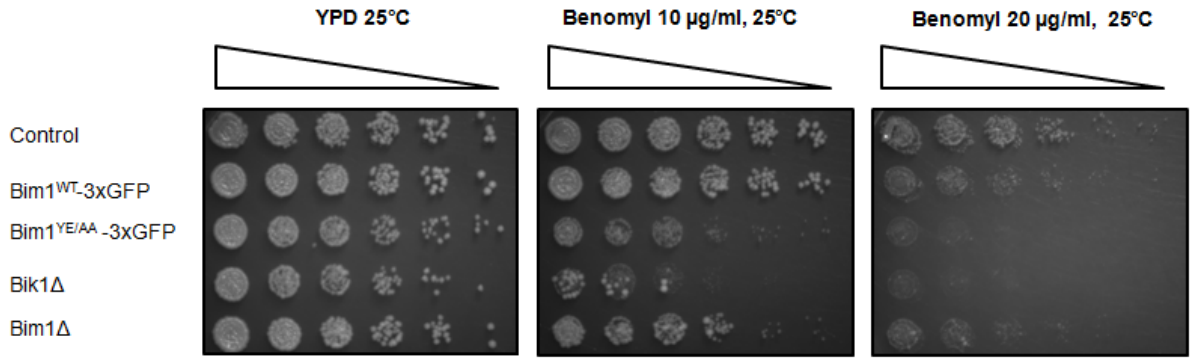

Figure 11. Testing Bim1 mutants having the known interaction motifs mutated for growth defects.

Different Bim1 variants were tested for growth defects on normal medium (YPD) and sensitivity to the MT destabilizing drug benomyl. Serial dilutions (1:4) of equal numbers of cells were spotted onto the indicated plates. Bik1Δ served as a positive control for benomyl sensitivity, DDY904, the background strain for the Bim1 variants, was used as a control strain.

4.2.2 Determination of the phenotype of a cargo deficient Bim1 mutant by live cell imaging

Next I aimed to analyze the localization of wild-type and cargo-deficient Bim1 in cells and investigate the effects on the MT skeleton. Using time-lapse live cell microscopy, MTs were visualized by expressing mCherry-tubulin. Bim1 versions were labelled C-terminally with 3xGFP. Looking at the cargo deficient mutant in unbudded cells, there were no striking changes of the MT cytoskeleton detectable. The number of MTs in the cell did not appear to be affected and the localization of Bim1 (to plus-ends of cytoplasmic and nuclear microtubules) seemed comparable in the Bim1^{WT}-3xGFP and the Bim1$^{YE/AA}$ -3xGFP strain. It should be noted that no quantitative analysis of MT dynamics was done, so more subtle alterations of MT dynamics per se cannot be excluded.

When imaging cells in mitosis, in most cases proper spindle elongation occurred with Bim1 loacalizing preferably at the midzone and also at astral MTs (Fig. 12). Again it should be mentioned that spindle elongation kinetics as well as spindle length was not determined. However, in anaphase, cargo deficient Bim1 mutant cells displayed clearly visible

phenotypes. More than 20% of the mutant cells had an elongated misoriented spindle (Fig. 13). Out of 40 WT cells in anaphase none showed this phenotype. A Bim1 deletion strain showed the same defect with similar quantity. Additionally, the spindle in cells of the cargo deficient mutant tends to display so called “rocking”, meaning that the spindle rotates or moves abruptly into opposite directions. This phenotype can also be observed in Bim1 deletion strains and is the consequence of compromised MT interactions with the cell cortex.

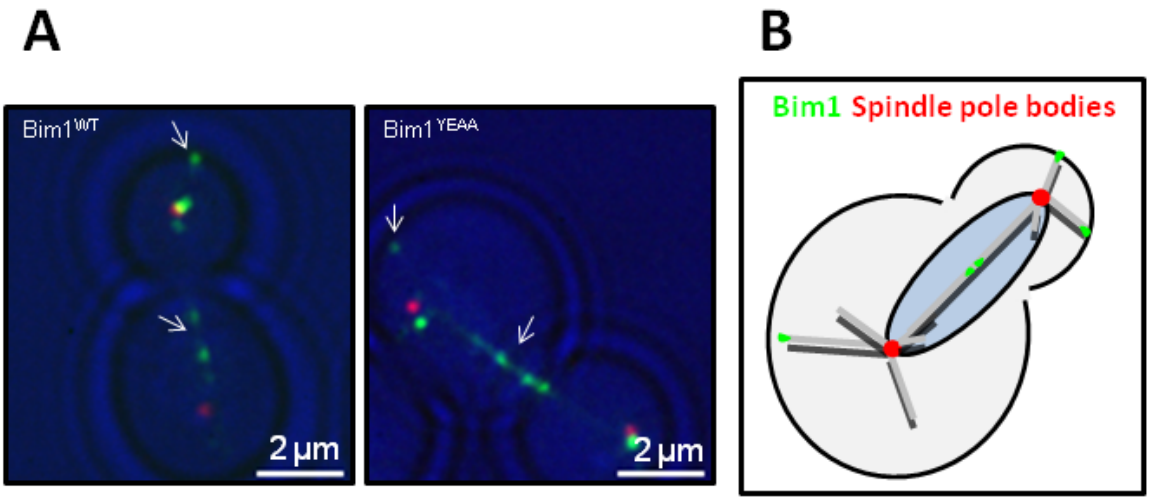

Figure 12. Localization of the Bim1 mutant during Mitosis.

(A) Live cell imaging using endogenously tagged Bim1 proteins**.** Bim1 is tagged with 3xGFP at the C-terminus; Spc42, which was used to visualize spindle pole bodies, is tagged with mCherry. Arrows indicate Bim1 localization at the spindle midzone and on growing astral microtubules.
(B) Cartoon of Bim1 localization during mitosis. During anaphase the mitotic spindle elongates and the chromosomes segregate. Bim1 always localizes at the spindle midzone, where MT plus ends overlap and on growing astral MTs.

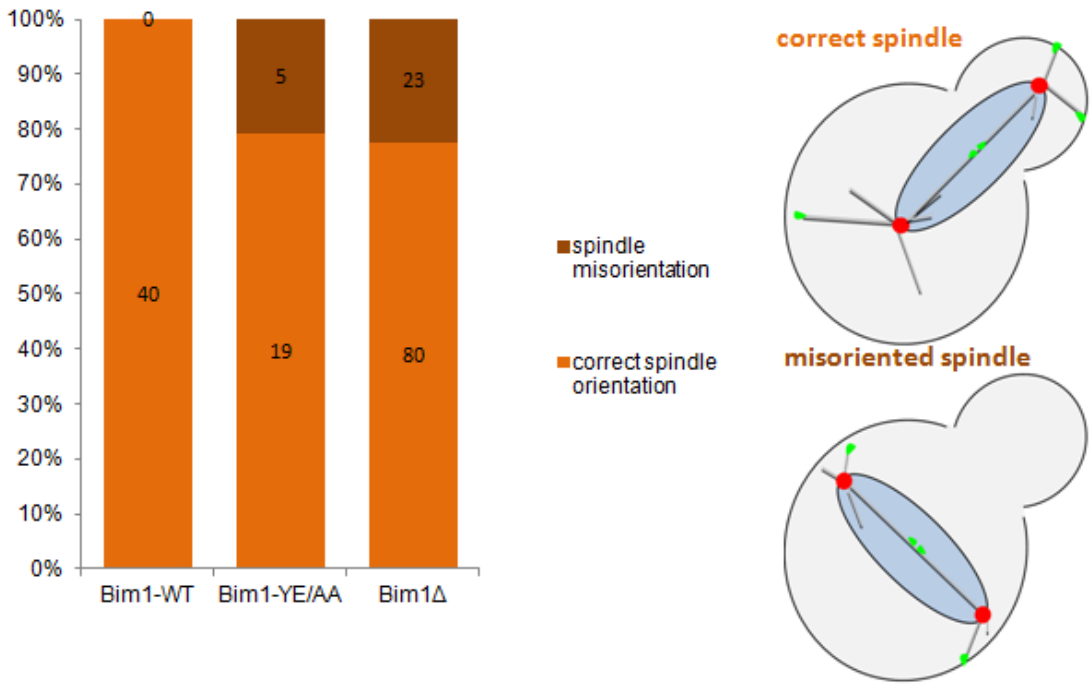

Figure 13. Analysis of the spindle orientation defect.

Quantification of the spindle misorientation defect. Model of correct spindle orientation and spindle misorientation in budding yeast, Spindle pole bodies are in red, Bim1 in green. Only cells that had an elongated spindle were taken for quantification.

4.2.3 The cargo deficient Bim1 mutant has an increased doubling time

The spindle misorientation defect occurred in around 20% of cells in the cargo deficient mutant and this might affect the doubling time. Therefore, it was quite surprising that there was no phenotype detectable by the spot assays on control medium. The spot assay may not be sensitive enough to detect small variations in doubling time. That is why I analysed the doubling time of the cargo deficient mutant in liquid cultures during exponential growth-phase. Indeed the mutant grew ~13% more slowly than the WT strain (Fig. 14). Interestingly the deletion strain seemed to perform slightly better compared to the mutant.

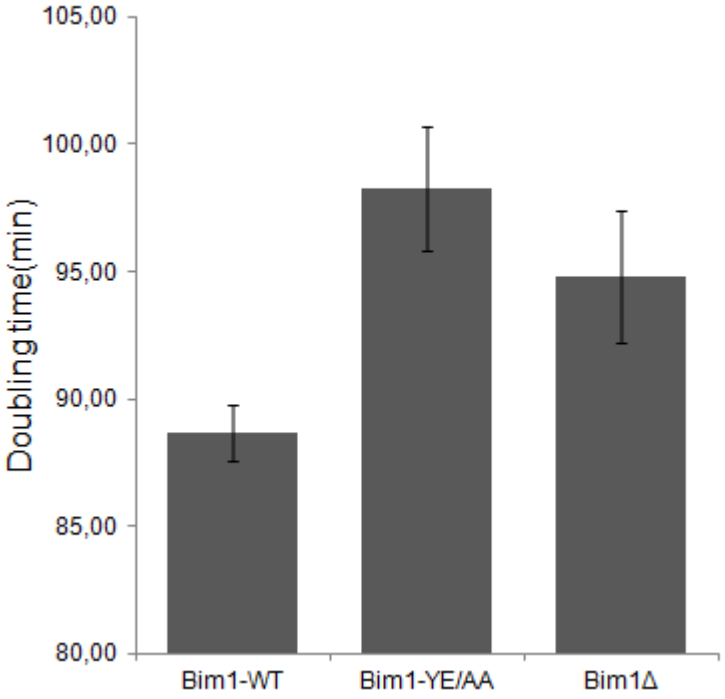

Figure 14. Determination of the doubling time of different Bim1 mutants during exponential growth.

Data was obtained from three independent experiments; in every experiment 3 samples of each strain were measured, making a total of 9 samples per strains. Doubling time was determined by measuring OD_{600}.

4.3 Detailed analysis of selected Bim1-Cargo interactions

4.3.1 Interaction between Bim1 and Nup159

For the identification and characterization of new Bim1 interaction partners selected proteins were chosen, which were then investigated more closely. The first one was Nup159, which is part of the nuclear pore complex (NPC), a multi-protein complex important for bidirectional nucleocytoplasmic transport. NPCs show a broad degree of compositional and structural conservation among all eukaryotes. Nup159 is an essential protein and localizes at the cytoplasmic side of the NPC [102]. The protein contains FG-repeats (Phenylalanine-Glycine repeat), which indicate that it has a direct function in transport. In the lab Babet van der Vaart and Alexander Schleiffer have already performed a bioinformatics screen searching for proteins that contain SxIP motifs. Nup159 was one of the most promising hits, having two motifs located in a flexible segment following a coiled coil domain. Colocalisation of Nup159-GFP with spindle pole bodies and IP Western blots indicated interaction between Bim1-FLAG or GST-Bim1 with Nup159-HA in vivo (Babet van der Vaart, personal communication).

However, it should be noted that in none of my mass spectrometry samples, peptides for Nup159 were found.

My aim was to investigate if the interaction between Bim1 and Nup159 is mediated by the EBH domain and the SxIP motifs in the two respective proteins. That is why strains having both SxIP motifs mutated were generated and in vivo pull downs were performed. The isoleucines and prolines in the motifs were replaced by two very polar amino acids, namely two asparagines. Honnappa et al. (2009) showed that these substitutions are sufficient to abolish binding of EB1 to MACF. Surprisingly these mutations did not seem to have an effect on the interaction between Nup159 and Bim1 (Fig. 15A). This indicated that Bim1 and Nup159 do not interact via the predicted motifs. To confirm this, I decided to perturb the interaction by using the Bim1 mutant that has the EBH domain mutated. However, there was again no reduced interaction detectable (Fig. 15B).

As the interaction between Nup159 and Bim1 could not be abolished, I tried to focus on other proteins.

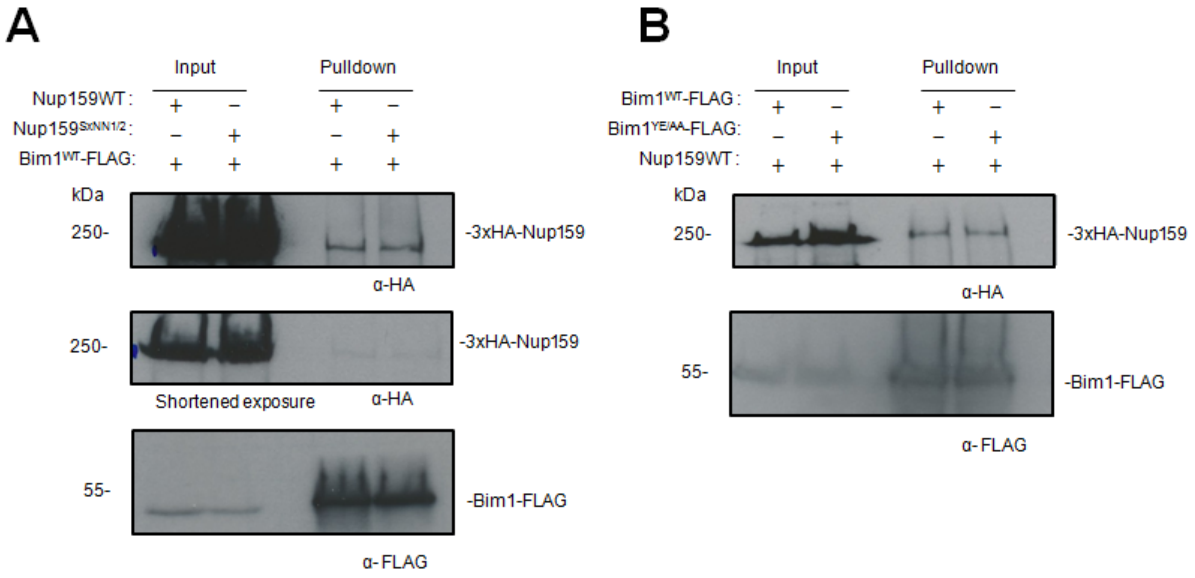

Figure 15. Testing the interaction between Nup159 and Bim1 variants.

(A) Testing the ability of Bim1^{WT}-FLAG to pull down Nup159$^{SXNN1/2}$ in vivo.
(B) Testing the ability of Bim1$^{YE/AA}$-FLAG to pull down Nup159 ^{WT} in vivo.

.

4.3.2 Interaction between Bim1 and Bck1

Next I investigated the interaction between Bim1 and Bck1. Bck1 is a MAPKKK acting in the protein kinase C signalling pathway, which is implicated in cell growth and controlling the cell wall integrity [103]. Upon activation by Pkc1p, Bck1 phosphorylates the redundant downstream MEK-kinases Mkk1p and Mkk2p. In yeast cells, Bck1 localizes to the tips of small buds[104].

The protein was also found in Bim1-FLAG pull downs followed by mass spectrometry analysis (Van der Vaart, personal communication). Moreover, sequence analysis revealed that the protein contains an SxIP motif and a LxxPTP sequence. The latter motif was recently discovered to be important in Kar9 binding to Bim1 (Diss. ETH No. 21563). Furthermore, GFP-Bck1 plus-end tracks/localizes to MTs in mammalian COS-7 cells (collaboration Ilya Grigoriev/Akhmanova lab).

Therefore, I again aimed to abolish the interaction by using the Bim1$^{YE/AA}$-FLAG mutant. By in vivo pull downs followed by western blot analysis there was no detectable difference between the amounts of Bck1 binding to Bim1^{WT}-FLAG and Bim1$^{YE/AA}$-FLAG (Fig. 16). It should be noted that in agreement with this result, I could also detect Bck1 peptides by mass spectrometry analysis, when pulling on Bim1$^{YE/AA}$-FLAG (Fig. 6B). As the interaction between Bck1 and Bim1 could not be abolished, I tried to focus on other proteins.

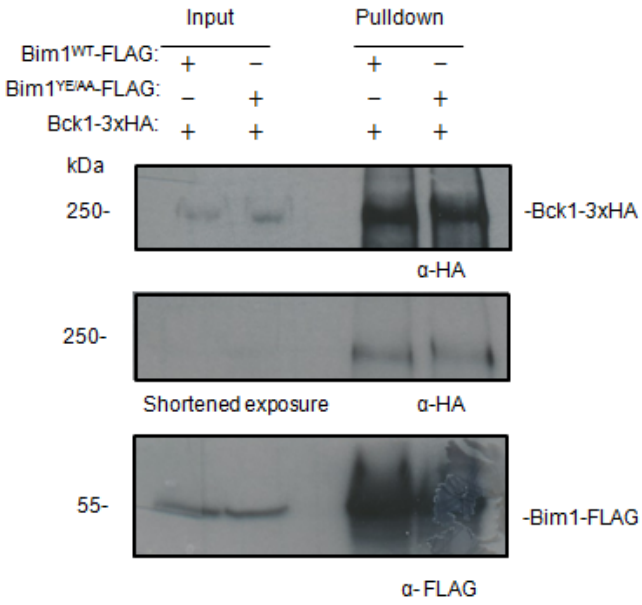

Figure 16. Testing the interaction between Bck1 and Bim1.

Investigating the ability of Bim1$^{YE/AA}$-FLAG to pull down Bck1^{WT}3x-HA in vivo.

4.4 Interaction between Bim1 and Ase1

The next protein that was selected for closer investigation was Ase1, a MAP that belongs to the conserved PRC1/ Ase1/MAP65 family and bundles antiparallel MTs. Due to its function as an MT crosslinker, it has an essential role in building up the spindle midzone.

The protein was also found in Bim1-FLAG pull downs followed by mass spectrometry analysis (Van der Vaart, personal communication). It contains two SxIP motifs at the N-terminus of the protein (Fig. 17C). In addition to that, it has been reported that the localization

of Bim1 to the spindle midzone depends on Ase1 [42]. The prediction would be that Bim1 and Ase1 bind each other via the SxIP sequence motifs and the EBH domain in the respective proteins (Fig. 17A). I used two approaches to manipulate the interaction; first I used the Bim1 mutant that had the EBH domain mutated. Indeed, as judged by Co-IP Western blot analysis, the association was reduced in comparison to WT by about three fold (Fig. 17B). Next I tried to disrupt the interaction by mutating the interaction site in Ase1, replacing the isoleucines and the prolines in the SxIP motifs to asparagines.

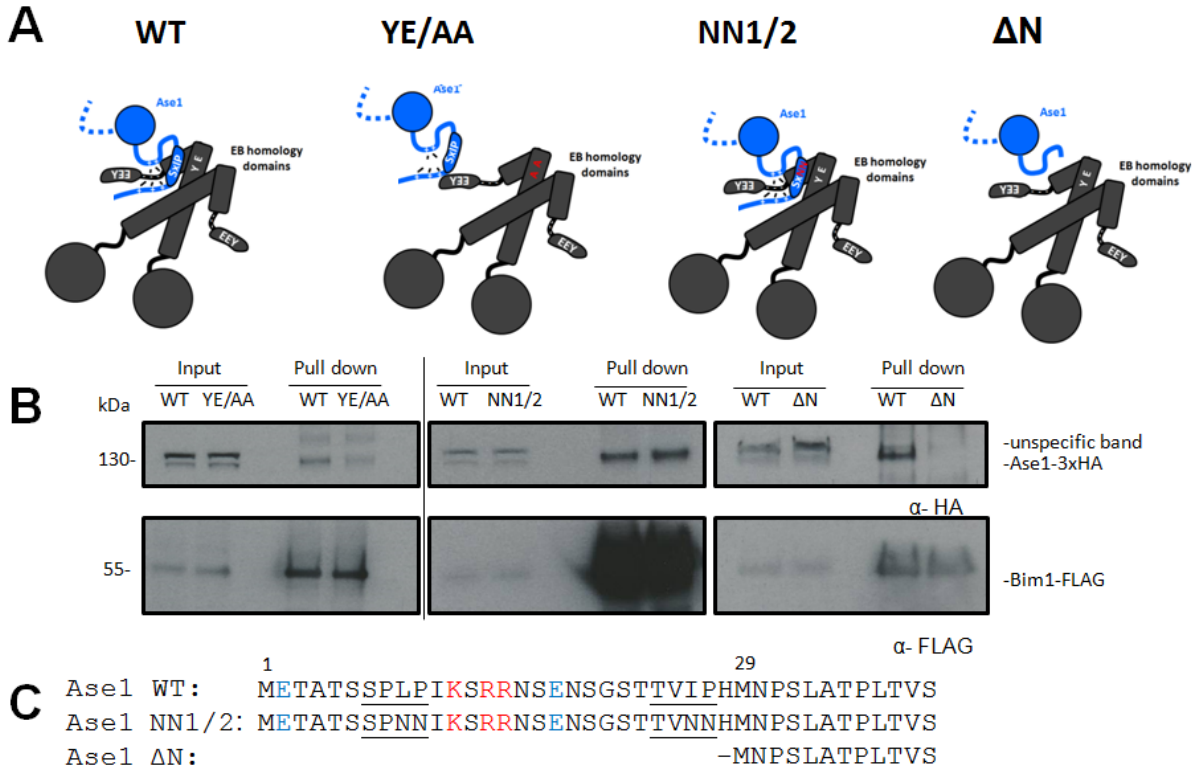

Figure 17. Investigating the interaction between Ase1 and Bim1.

(A) Model of Ase1 binding to Bim1.
(B) In vivo FLAG pull downs followed by western blot analysis. WT= $Bim1^{WT}$-FLAG, YE/AA=$Bim1^{YE/AA}$ -FLAG, NN1/2=$Ase1^{NN1/2-HA}$, ΔN =$Ase1^{\Delta N-HA}$.
(C) Sequence alignment of Ase1 constructs

Surprisingly these mutations did not have an effect on binding (Fig. 17B). As mentioned in the introduction, there are usually extensive salt bridges formed by the basic residues surrounding the SxIP motifs and the acidic amino acids next to the EBH domain that support binding. Therefore I generated an Ase1 mutant that lacked a small part of the N- terminus, including both SxIP motifs and some positively charged amino acids. The N-terminal part of the protein is required for dimerization but the two SxIP motifs are still positioned in the unstructured region of the N-terminus that should still be outside of the dimerization region. Deletion of the N-terminal part of Ase1 abolished the binding to Bim1 in vivo (Fig. 17B), indicating that this part is required for the interaction.

4.4.1 The N-terminal domain is required for proper Ase1 function in vivo

In vivo pull downs showed that removing the N-terminal part, containing the two SxIP motifs, of Ase1 results in a reduced interaction between Ase1 and Bim1, but the functional importance of that interaction was unclear. In order to test if cells, in which the interaction is abolished, display a growth phenotype, I performed spotting assays. On rich YPD medium no growth defect was detected (Fig. 18). However, the Ase1ΔN mutant displayed increased sensitivity to benomyl, indicating that there is a role for the interaction between Bim1 and Ase1 in organizing or regulating the MT cytoskeleton.

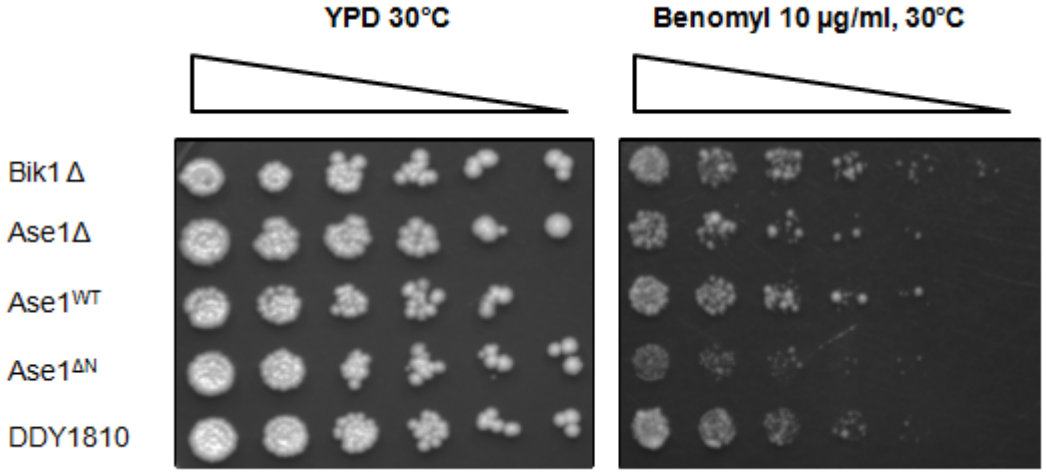

Figure 18. Testing the Ase1$^{\Delta N}$ mutant for growth defects.

Ase1$^{\Delta N}$-3xHA mutant was tested for growth defects on normal medium (YPD) and sensitivity to the MT destabilizing drug benomyl. Serial dilutions (1:4) of equal numbers of cells were spotted onto the indicated plates. Bik1Δ served as a positive control for benomyl sensitivity, DDY1810, the background strain for Ase1^{WT} and Ase1$^{\Delta N}$, was used as a reference strain. It should be noted that Ase1Δ and Bik1Δ were in the DDY904 background, which in general grows better than DDY1810.

4.4.2 Investigating the interaction between Ase1 and Bim1 in vitro

Co-IP experiments indicated an interaction between Bim1 and Ase1 in cell extracts. In order to investigate the molecular basis for the interaction and determine whether the proteins engage in a defined complex I sought to express and purify both proteins. GST-Bim1 ^{WT} was already available in the lab (work done by Tomasz Zimniak). I purified GST-Bim1$^{YE/AA}$ from bacteria according to materials and methods.

4.4.3 Purification of Ase1 from yeast cells and insect cells

It should be mentioned that I also aimed to purify Ase1-STREP from a BL21 DE3 *E.coli* strain. For that purpose Ase1-STREP was cloned into the pet28a+ vector. By using 1 mM IPTG and induction O/N at 18°C no induction of protein expression was detectable neither by SDS-page and Coomassie staining nor by western blotting.

To circumvent the difficulty that high molecular weight proteins are often not expressed in bacteria, I initially used the galactose inducible overexpression system in yeast. Purification of 1xFLAG-Ase1-HALO from a two-micron plasmid under the control of the pGAL promoter resulted in the purification of soluble Ase1, but the protein yield was not sufficient for extended biochemical experiments (Fig. 19).

To increase the amount of protein I took advantage of the Baculovirus insect cell Expression System, which had been already established in the lab. Indeed the amount of protein that can be purified from insect cells is much higher (Fig. 19).

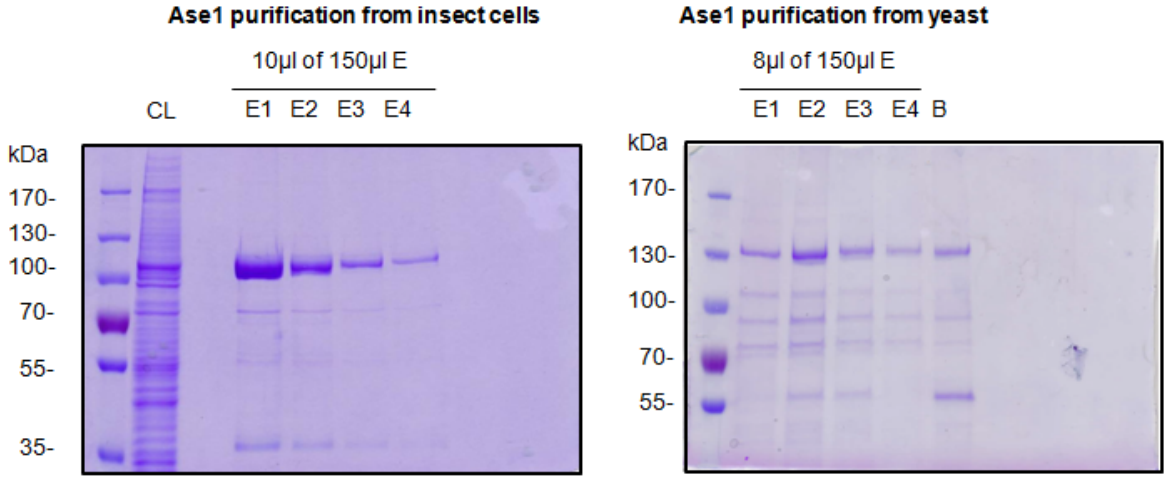

Figure 19. Expression and purification of Ase1 from different organisms.

The left gel displays the consecutive elution fractions with desthiobiotin, when purifying Ase1 from insect cells. 200 ml of insect cells were transfected and used for this purification. On the right side the elutions achieved from a budding yeast sample are shown. The protein was purified from 5 litres of budding yeast culture. Differently tagged Ase1 was used in both organisms. Ase1 that was purified from insect cells was STREP tagged C-terminally, while FLAG-Ase1-HALO was purified from yeast cells. This led to the different protein sizes on the gel, ~100kDa in insect cells, ~130kDa in budding yeast. CL=cleared lysate; B=beads after elutions.

4.4.4 Ase1 purified from insect cells binds MTs in a cosedimentation assay

To determine the functionality of the recombinant Ase1 I carried out an MT cosedimentation assay. Ase1-STREP bound to MTs in a concentration dependent manner with a dissociation constant of 0.23 µM (Fig. 20A/B). This value is in the range of dissociation constants reported for PRC1 proteins in the literature [31].

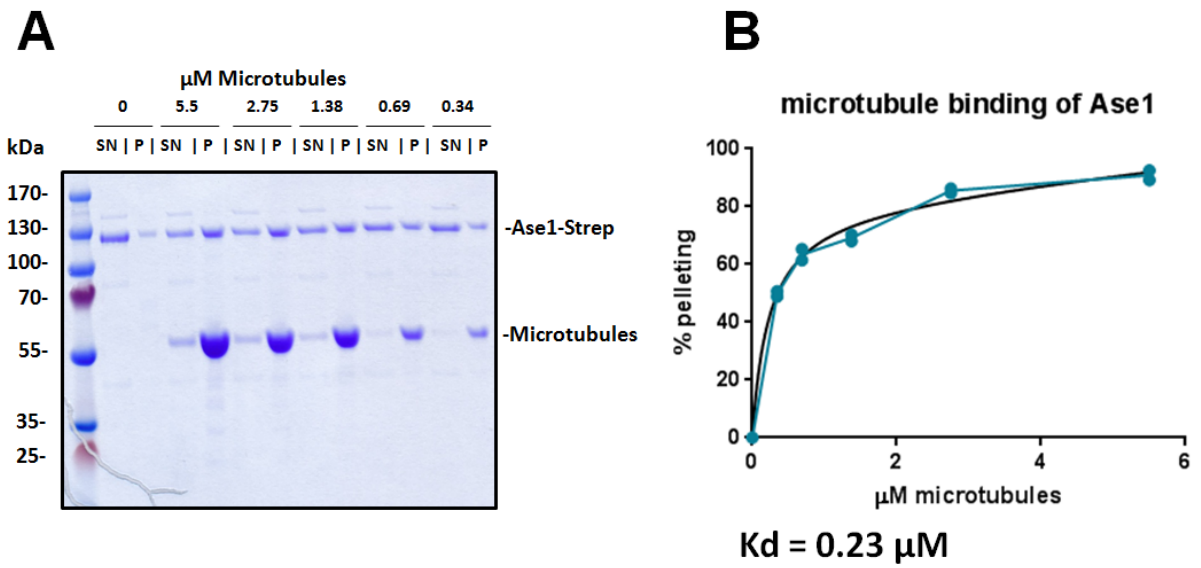

Figure 20. Ase1-STREP binds microtubules in a cosedimentation assay.

(A) Ase1-STREP purified from insect cells was incubated with varying concentrations of taxol stabilised MTs and centrifuged. Supernatant (S) and pellet (P) are divided and separately analysed by SDS-PAGE. A sample containing no MTs was used as a negative control.
(B) Graph displaying the percentage that binds to MTs at varying concentrations. For the determination of the Dissociation constant two independent experiments were used. The black line displays the fitted curve, the blue line shows the mean values of the two experiments.

4.4.5 Ase1 directly interacts with Bim1 via the EBH domain

As indicated by pull-downs from yeast extracts Ase1 and Bim1 associate with each other in vivo (Fig. 17B). To verify that the interaction is indeed a direct one and not mediated via other proteins I used purified recombinant proteins and performed in vitro pull downs. In these experiments Ase1 binds to Bim1 in a concentration dependent manner (Fig 21A). Moreover size exclusion chromatography (SEC), which is a more stringent way to show an interaction between two or more proteins, was performed. Even under high salt conditions (300 mM NaCl) a stable complex between the two proteins is formed (Fig. 22A/B).

After showing that both proteins bind each other directly I wanted to map the interaction interfaces. In vivo, I could already show that the EBH domain of Bim1 was required for the interaction. In vitro, Bim1$^{YE/AA}$ showed again significantly reduced binding to Ase1, proving that it is indeed the EBH domain that mediates binding (Fig 21B).

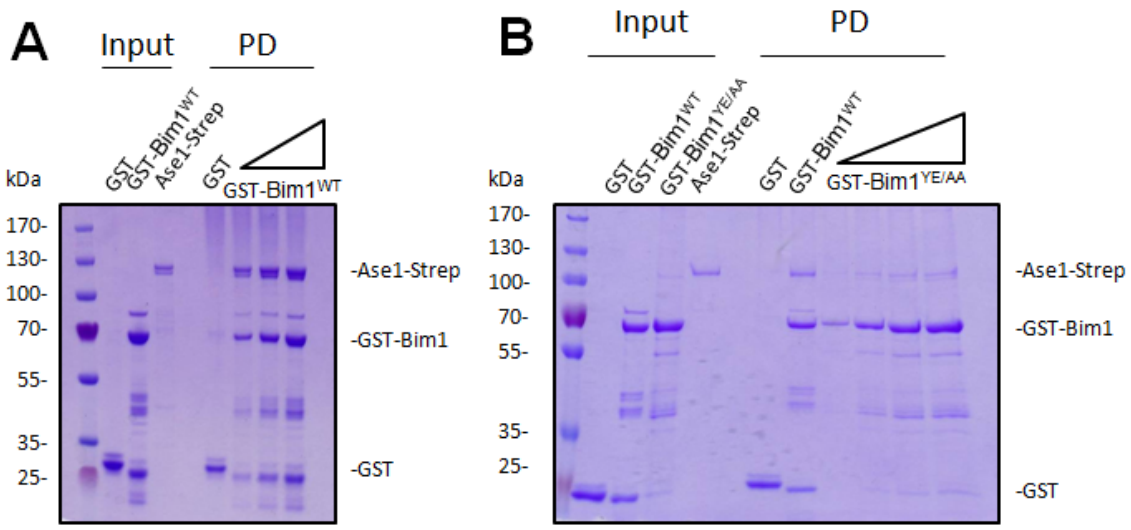

Figure 21. Ase1 directly interacts with Bim1 via the EBH domain.

(A) Ase1-STREP binds to GST-Bim1 in a concentration dependent manner. Proteins were incubated with glutathion-sepharose beads, removed from the beads by boiling in SDS sample buffer and analysed by SDS-PAGE. The concentration of Ase1-Strep was kept equal, while GST-Bim1 concentrations were varying. As a negative control GST alone was used. As input 10% of Ase1-STREP was loaded. Pull-downs were performed in 25 mM Hepes pH 8.0, 150 mM KCl buffer. Samples were analysed by SDS-PAGE and Coomassie staining.
(B) The GST-Bim1$^{YE/AA}$ mutant is very inefficient in pulling down Ase1-STREP compared to GST-Bim1^{WT}. Proteins were incubated with glutathion-sepharose beads, removed from the beads by boiling in SDS sample buffer and analysed by SDS-PAGE. The concentration of Ase1-Strep was kept equal, while GST-Bim1 concentrations were varying. GST alone was used as a negative control. 10% of Ase1-STREP was loaded in the input. Pull-downs were performed in 25 mM Hepes pH 8.0, 150 mM KCl buffer. Samples were analysed by SDS-PAGE and Coomassie staining.

4.4.6 The N-terminal region of Ase1 is not required for binding to Bim1 in vitro

Next I wanted to define the region necessary for binding Bim1, in Ase1. As shown above, the in vivo data suggested that it is the extreme N-terminal region that mediates binding. I purified recombinant Ase1 lacking the N-terminus and tested its ability to bind Bim1 via SEC. Quite surprisingly under the used experimental setup Ase1$^{\Delta N}$-STREP and GST-Bim1 formed a stable complex (Fig. 22A/B). Both, Ase1^{WT} and the mutant interacted with GST-Bim1 in a ~1:1 stoichiometry. The N-terminal part, containing the two SxIP motifs, is not required for

binding to Bim1, at least in vitro. To test whether the affinity of the interaction might be reduced, I performed an in vitro pull down assay with varying Bim1 concentrations. The amount of Ase1^{WT}-Strep and Ase1$^{\Delta N}$-Strep was kept equal. In this assay again no difference in binding between the WT and the mutant protein was detected (Fig. 23). It is possible that the Ase1 concentration used in this assay was too high for detecting a difference in binding affinity. In order to avoid that the Ase1 concentration is saturating one could vary in future experiments the Ase1^{WT}-Strep and Ase1$^{\Delta N}$-Strep concentration, while keeping GST-Bim1 constant.

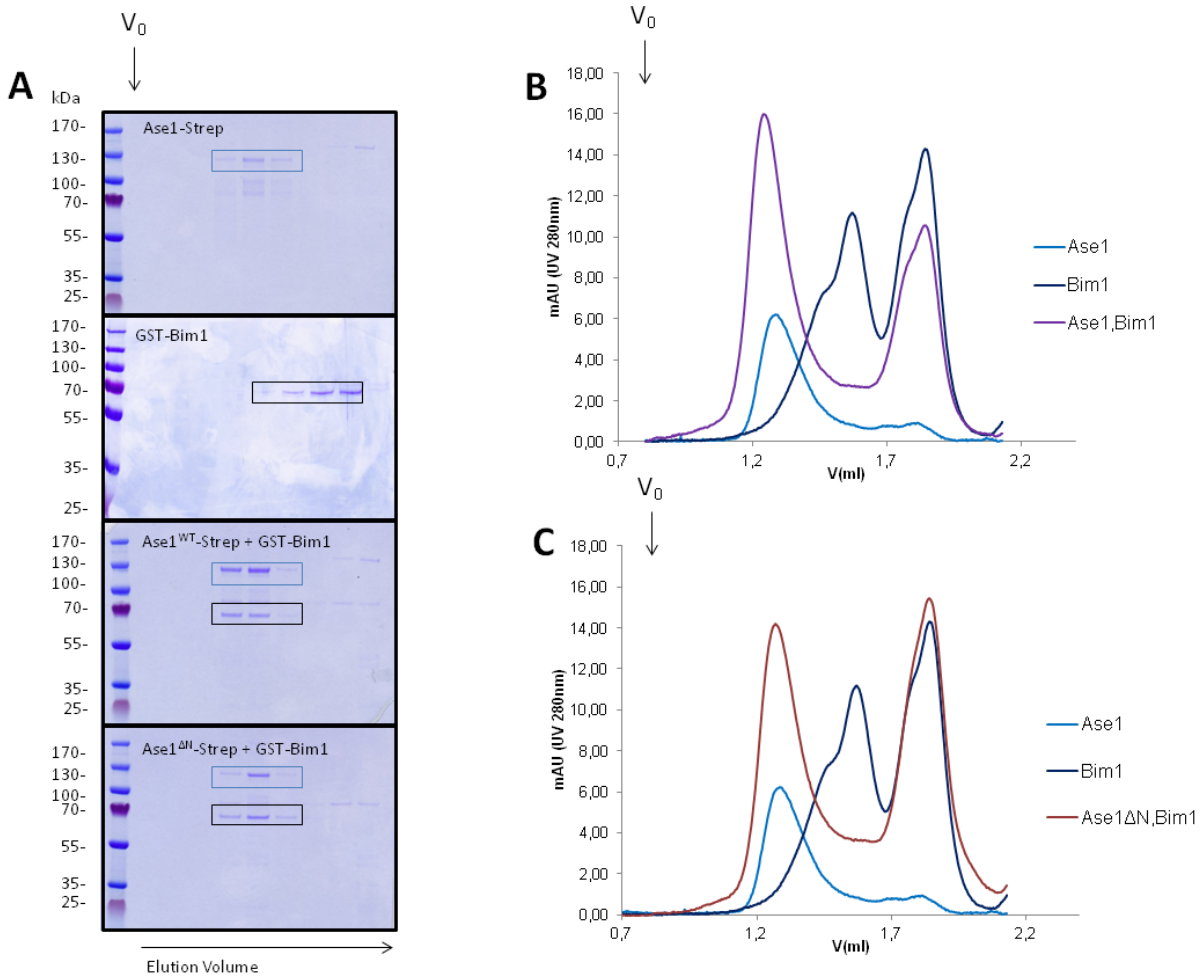

Figure 22. Size exclusion chromatography analysis of Bim1-Ase1 complexes.

Gel filtration was performed in NaH_2PO_4 pH 8, 300mM NaCl, Buffer on a Superose 6 column. Samples were analysed by SDS-PAGE and Coomassie staining.

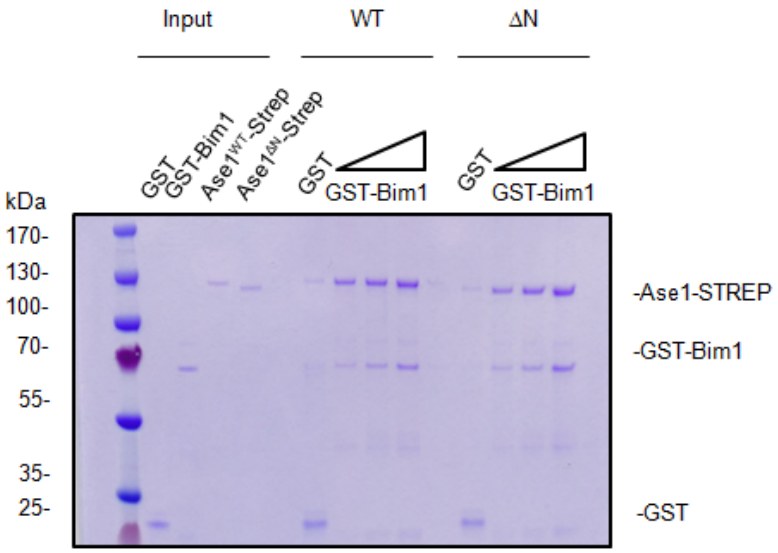

Figure 23. Ase1 lacking the N-terminal part shows no reduced binding to Bim1.

Proteins were incubated with glutathion-sepharose beads, removed from the beads by boiling in SDS sample buffer and analysed by SDS-PAGE. The amounts of Ase1 were kept equal in the pull-downs, while different quantities of GST-Bim1 were used. GST alone was used as a negative control. 10% of Ase1-STREP was used for the input. Pull-downs were performed in 25 mM Hepes pH 8.0, 150 mM KCl buffer. Samples were analysed by SDS-PAGE and Coomassie staining.

4.4.6 TIRF microscopy analysis of Ase1 and Bim1

Bim1 and Ase1 both localize at the spindle midzone during mitosis and play a crucial role in forming a proper spindle [91] [31]. Ase1´s ability to bundle antiparallel MT arrays makes it crucial for spindle elongation and stabilization. Deletion of Ase1 gives rise to small spindles and increases the probability of spindle collapse [31]. The role of Bim1 in spindle morphogenesis is less clear but deletion phenotypes demonstrate its importance in this process. Bim1 deletions display decreased elongation speed in anaphase, and shortened spindles [79].

Now that we found that these two conserved proteins interact with each other directly a couple of questions arise. What is the function of the interaction, does it play a role in spindle formation? How does the presence or absence of one protein change the behaviour of the other one?

To start addressing these questions I first aimed to analyze the individual and combined interaction properties of Ase1 and Bim1 with microtubules by TIRF microscopy, which enables the detection of fluorescently labelled molecules with high sensitivity.

4.4.7 Bim1 promotes recruitment of Ase1 to taxol-stabilized microtubules in vitro

Before using dynamic MTs I wanted to image Bim1 and Ase1 interacting with stable MTs. Coverslips in the microscopy flow chamber were coated with α-tubulin antibody. After the attachment of taxol stabilised MTs, unbound MTs were washed away. Finally, the labelled proteins of interest were flown in and observed (Fig. 24B). Ase1 and tubulin was labelled as explained in materials and methods, Bim1-eGFP was already available in the lab (work done by Tomasz Zimniak).

First Ase1's interaction with individual microtubules was visualized. Interestingly it was not binding to MTs under the used conditions (Fig. 24A), whereas Bim1 strongly associated with the lattice of taxol stabilized microtubules. This might seem surprising, given the fact that Ase1 binds MTs in cosedimentation assays. An explanation for this behaviour is that due to the long incubation step of Ase1 with taxol stabilised MTs in the cosedimentation assay, Ase1 is able to bundle and bind to antiparallel MTs. In the TIRF-setup taxol stabilised MTs are already attached on the coverslip, when Ase1 is floated in. Therefore, no antiparallel MTs, to which Ase1 could bind to, are formed. The affinity of Ase1 for individual, non-bundled, microtubules may not be sufficiently high to observe binding under these conditions. Interestingly, upon inclusion of Bim1, Ase1 was readily observed associating with single microtubules (Fig. 24A). This shows that Bim1 can target Ase1 to MTs, when Ase1 alone would not be able to associate with MTs.

Recruitment by Bim1 was retained when I used the $Ase1^{\Delta N}$ mutant instead of $Ase1^{WT}$ (Fig. 24C), a further indication that the N-terminal region is not required for binding of Ase1 to Bim1 in vitro.

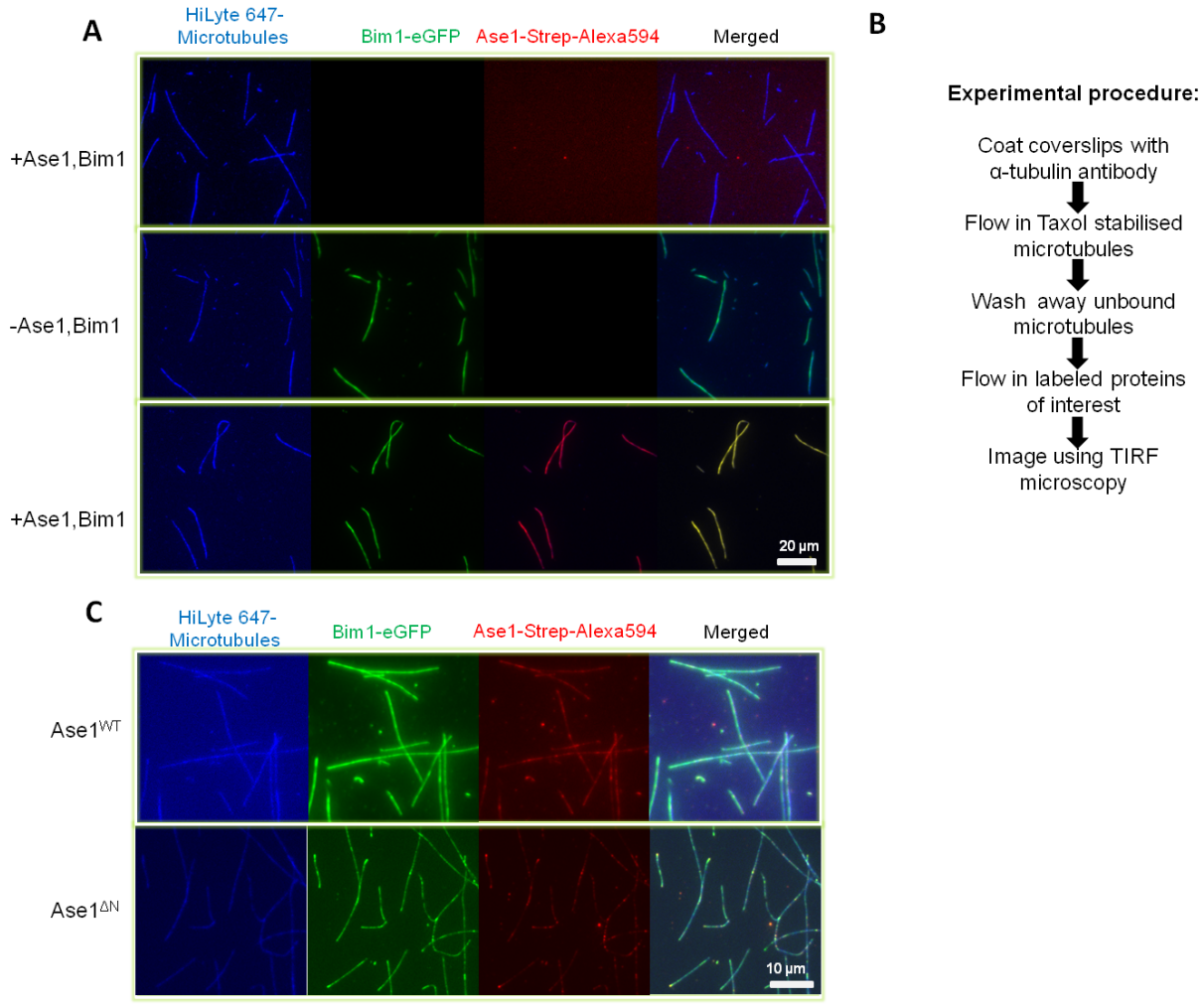

Figure 24. Bim1-eGFP recruits Ase1-STREP-Alexa594 to taxol stabilized microtubules.

(A) Bim1 recruits Ase1^{WT} to taxol stabilised MTs. Imaging was done at 30°C and 66 mM KCl using total internal reflection microscopy. MTs were sparsely labelled with HiLyte 647.
(B) Schematic of the experimental procedure for (A) and (C)
(C) Bim1 also recruits Ase1$^{\Delta N}$ to taxol stabilised MTs. Imaging was done at 30°C and 66 mM KCl using total internal reflection microscopy. MTs were sparsely labelled with HiLyte 647.

4.4.8 Ase1 binds preferentially to microtubule bundles

To ask whether Ase1 can bind antiparallel MTs in this experimental approach, we changed the experimental procedure. Prior to flowing in the sample, the proteins of interest were incubated with taxol stabilized MTs for 40 minutes. Under these conditions Ase1-Strep-Alexa594 alone localizes exclusively to subsets of MTs, characterized by an increased fluorescence signal in the microtubule. These microtubule segments constitute bundles, probably corresponding to antiparallel microtubules (Fig. 25).

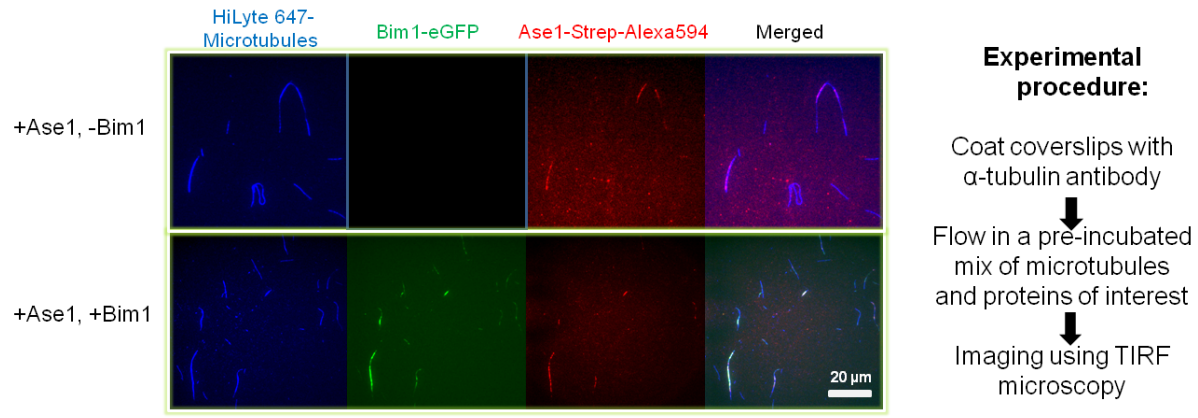

Figure 25. In the absence of Bim1, Ase1 preferably associates with bundled microtubules.

Imaging was done at 30°C and 66 mM KCl using total internal reflection microscopy. MTs were sparsely labelled with HiLyte 647. On the right side the schematic of the experimental procedure is depicted.

4.4.9 Analysis of Ase1 and Bim1 in combination with dynamic microtubules

In living cells MTs are highly dynamic, this property can be recapitulated in vitro with a variation of the assay described above: First the biotinylated coverslips in the microscopy flow chamber were coated with avidin. Rhodamine-labeled, biotinylated GMPCPP-MT seeds were attached to the surface by binding to avidin. Unbound seeds were washed away. Next, free and dimly labelled HiLyte 647-tubulin was added, in the presence of proteins of interest, to allow MT growth.

With this setup, I could reconstitute plus end tracking of Bim1 (Fig. 26). The effect of Bim1 on the association of Ase1 with dynamic microtubules could not be assessed, as inclusion of higher concentrations of Ase1 abolished plus end tracking of Bim1, an effect that was apparently caused by a property of the Ase1 storage buffer. Including low concentrations of Ase, which would still enable plus end tracking of Bim1, was not sufficient to visualize Ase1 on the dynamic microtubules. To assess if Bim1 can recruit Ase1 to growing microtubule plus-ends, a further optimization of the purification and imaging conditions is required.

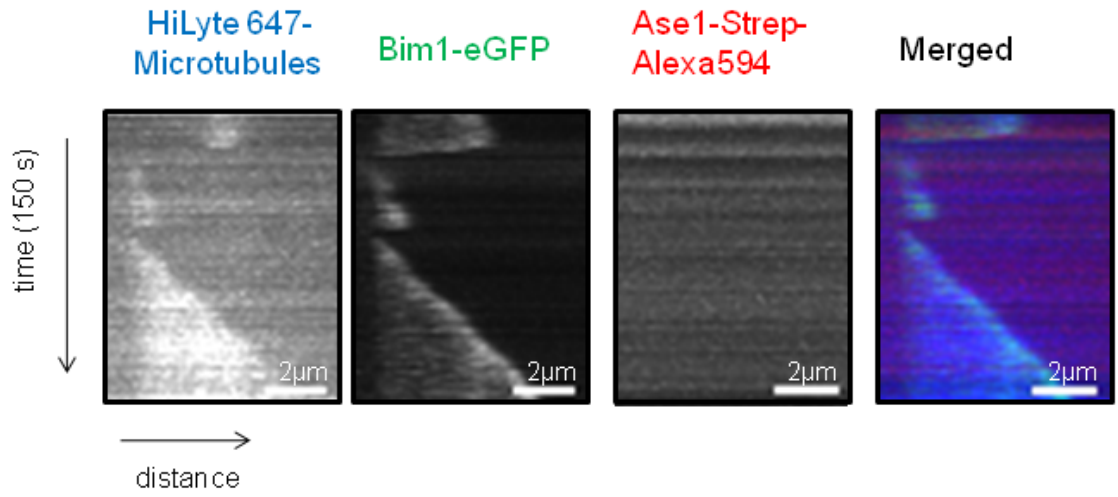

Figure 26. Investigating the collective behavior of Bim1 and Ase1 on dynamic microtubules.

Imaging was performed at 30°C with a final concentration of 175 mM KCl in the imaging buffer using total internal reflection microscopy. MTs were sparsely labelled with HiLyte 647.

4.4.10 Ase1 and Bim1 localize independently from each to the spindle midzone

As already mentioned above, it was stated in the literature that Bim1 spindle midzone localization depends on Ase1, as in an Ase1 deletion strain Bim1 was not detected at the midzone anymore [42]. Therefore, one would expect that the cargo deficient Bim1 mutant which is not interacting with Ase1 anymore is also removed from the spindle midzone. However, when I performed live cell imaging with endogenous fluorescently tagged proteins Bim1$^{YE/AA}$-3xGFP localized to the spindle midzone with a pattern and intensity that was similar to the wild-type protein (Fig. 27). Confirming this observation, Bim1 localization was retained in an Ase1 deletion strain that I constructed. There may be subtle differences in the Bim1 localization, as it did not seem as restricted to the midzone as in Bim1^{WT} or Bim1$^{YE/AA}$ strains.

I conclude that both proteins, Bim1 and Ase1, can localize independently from each other to the spindle midzone, contrary to what has been reported in the literature.

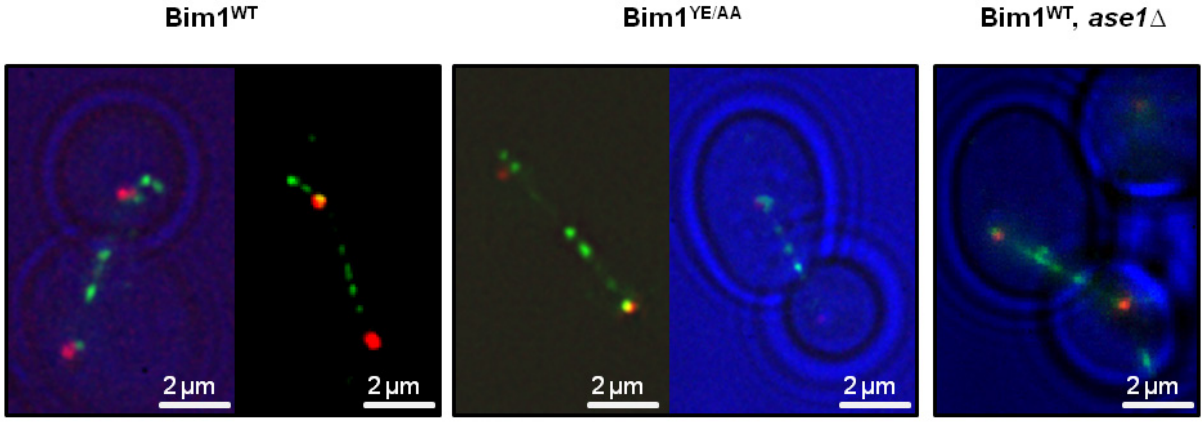

Figure 27. Localization of Bim1.

Live cell imaging using endogenously tagged Bim1 versions**.** Bim1 is tagged with 3xGFP at the C-terminus; Spc42, which was used to visualize spindle pole bodies, is tagged with mCherry.

5. Discussion

To understand the molecular mechanisms underlying the regulation of the MT cytoskeleton it is required to identify all proteins that are associated with MTs. End Binding (EB) proteins that potentially interact with all +TIPs are the central adaptors of MT tip associated networks. By generating a Bim1 (budding yeast EB1 homolog) mutant that is not able to target other proteins to the MT plus end, I have generated a tool that allows the separation of the direct and indirect effects of Bim1 on MT dynamics. In addition, I identified Ase1 as a new Bim1 (budding yeast homolog of EB1) interaction partner and investigated the molecular basis for the cooperation between plus end tracking and microtubule bundling proteins.

5.1 Comparison of different tagging strategies for Bim1

At the N-terminus Bim1 contains the CH-domain, which mediates binding to MTs, while the extreme C-terminus consists of an EEY/F motif that is required for binding CAP-Gly domain containing proteins. As shown in this study tagging Bim1 at either end is not unproblematic. Tagging at the N-terminus with a 6xHis/6xFLAG tag significantly reduced the amount of protein levels in cells (Fig 6C). So far it has been shown that tagging mammalian EB1 at the N terminus with a GFP tag leads to mislocalisation of the protein, away from MTs to other cytosolic compartments [97]. The same was observed when a smaller 14 aa long V5 tag was used, although the effect was less strong [97]. Contradictory to this data, the use of a 6xHis tag at the N-terminus even increases the affinity for MTs [105]. A possible explanation for this behaviour might be that the added positively charged aa might support the interaction with the largely acidic C-terminal tail of tubulin.

In this study a 6xHis/6xFLAG tag was used for in vivo pull-downs. In comparison to the 6xHis tag, the 6xHis/6xFLAG tag is only partially positively charged because each FLAG tag contains also five negatively and only two positively charged aa. Apart from that, also the size of the tag is increased. Although the size is smaller than a GFP tag, it might be already sufficient to function as a steric obstacle. Thus, most likely the interaction with MTs is rather decreased than enhanced by the N-terminal 6xHis/6xFLAG tag. The reduced ability to bind to MTs might target the majority of the protein to other cytosolic compartments and thereby making it more unstable, leading to reduced amounts of protein.

The fact that I was able to identify a lot of MAPs in the in vivo pull downs followed by mass spectrometry with N-terminal tagged Bim1 versions indicates that N-terminal tagged Bim1 at least partially localizes at MTs and that the interaction with tubulin is not completely abolished. Moreover if the N-terminal tagged Bim1 could not bind MTs at all, I probably

would not have seen a growth-defect of the EBH mutant in the spot-assay (Fig 11). To ascertain the localization of N-terminally tagged Bim1, one could perform live cell imaging with cells expressing mCherry-tubulin and FLAG-Bim1^{WT}-3xGFP.

As an alternative strategy, C-terminal tags were used in this study. At least for EB1 it was shown that a GFP tag at the C-terminus does not alter the localization of the protein. In this study, endogenously tagged Bim1^{WT}-3xGFP showed in comparison to the background strain increased sensitivity to high concentrations of benomyl. In mammalian systems it was already shown that a C-terminal GFP tag interferes with binding to the mammalian Bik1 homolog, CLIP-170 [97]. The loss of the Bim1-Bik1 interaction may have caused the phenotype in the spot-assay.

For further studies it might be interesting, although more complicated, to use internally tagged proteins. The flexible linker between the CH and the EBH domain might represent a suitable site. However, one would need to be careful that the internal tags do not alter sites of regulation, as the linker harbours known phosphorylation sites [79].

5.2 Phenotypes of a cargo deficient Bim1 mutant

5.2.1 Spindle positioning defect

The most obvious and striking phenotype of the cargo deficient Bim1 mutant was the spindle positioning defect. Cells had already elongated, misoriented spindles in anaphase and the spindle tended to display so called “rocking”, meaning that the spindle rotates or moves abruptly into different directions without aligning to the mother-bud long axis.

In budding yeast the mitotic spindle consists of two spindle poles that serve as nucleation sites for two distinct classes of MTs. One class are nuclear microtubules that form the mitotic and meiotic spindle and are required for chromosome segregation. The other class, called cytoplasmic MTs, is necessary for karyogamy, nuclear positioning and spindle orientation [106].

The current model for spindle orientation states that Kar9 is recruited by Bim1 to MT plus ends located at the bud neck. Next, a class V myosin called Myo2, associates with these astral MTs via directly interacting with Kar9 and pulls them along the actin filaments into the bud. Subsequently the MTs get attached to the cell cortex by Bud6 via unknown mechanisms. By actively shortening the MTs, while they stay captured at the cortex, the spindle gets further dragged into the future daughter cell [107].

As shown by the mass spectrometry analysis of in vivo pull-downs, the SxIP motif containing protein Kar9 was the most abundant binding partner of Bim1 in cells and the interaction was abolished by the mutations in the EBH domain.

The described spindle positioning pathway depends on the interaction between Kar9 and Bim1. Therefore, it is not surprising that the cargo deficient Bim1 mutant displays the observed defects in spindle orientation.

The reason why the mutant strain maintains its viability is probably due to the presence of a second partially redundant spindle orientation pathway. This pathway depends on the minus-end directed Dynein–Dynactin complex, a MT minus-end directed motor. Dynein localization to MT plus ends is achieved by its interaction with Bik1, which is actively transported to plus ends via Kip2. After reaching the cell cortex, dynein gets activated by Num1. Activated dynein pulls the spindle pole body into the bud via its minus end directed movement, while staying anchored at the cortex.

In budding yeast cell division despite the incorrect positioning of the spindle along the mother-bud axis can lead to aneuploidy. A surveillance mechanism known as the spindle position checkpoint (SPOC) prevents cells having a misoriented spindle from exiting mitosis [108]. I assume that in the cargo deficient mutant and the Bim1 deletion strain the SPOC delays the exit from mitosis by inhibiting the mitotic exit network leading to an increased doubling time.

5.2.2 Effects on microtubule dynamics

Live cell microscopy indicated that the cargo-deficient Bim1 mutant displayed normal plus-end localization in cells. Besides the obvious spindle orientation phenotype, there could additionally be more subtle changes in microtubule dynamics that could be investigated in further studies. Similar to a Bim1 deletion strain, MTs in the cargo deficient strain might display reduced dynamics including slower shrinkage rates, fewer rescues and catastrophes, and spending more time in paused state [73]. Closer investigations on the dynamics of MTs in the wild type, the cargo deficient mutant and the deletion strain would not only answer this question, but also shed some light on the direct effects of Bim1 on MT dynamics.

In the assays used in this study for analysing the growth and spindle orientation phenotype, the Bim1 cargo deficient mutant behaved quantitatively similar to a Bim1 deletion strain. Around 20% of cells in both strains displayed the spindle misorientation defect and the doubling time of the cargo deficient mutant was even higher than the one of the deletion strain. So in general the cargo deficient mutant showed no rescue effect compared to the deletion strain. Therefore, we argue that the more important function of Bim1 is to recruit other MAPs to the MT plus end compared to directly affecting MT dynamics. That is why it is important to find additional binding partners of Bim1 and analyse the interplay of these MAPs with each other.

5.3 Bim1 and Ase1 interaction interfaces

The in vivo and in vitro pull-downs clearly showed that Bim1 and Ase1 interact directly with each other. Additionally, as expected, all experiments performed in this study indicated that in Bim1 it is the EBH domain that mediates binding to Ase1.

Surprisingly Ase1, having the canonical SxIP interaction motifs mutated, was still efficiently pulled down by Bim1 in vivo. This was contrary to the expectation that the replacement of the two hydrophobic aa, isoleucine and proline by two polar asparagines would be sufficient to disturb the interaction with the hydrophobic cavities in the EBH domain. This raises the question what additional elements could contribute to the binding interface in Ase1?

As already mentioned also salt bridges between basic amino acids surrounding the SxIP motif and negatively charged aa next to the EBH domain usually contribute to binding. There are three positively charged amino acids (two arginines and one lysine) between the two nearby SxIP motifs that could enhance the interaction. But these salt bridges, although maybe participating in binding, should not be sufficient for it. Otherwise in the EBH mutant, where salt bridges are also not disrupted, Bim1 would still be able to bind to Ase1. So there might be other hydrophobic aa in Ase1 associating with the EBH domain.

The delta N mutant eliminates the SxIP motifs and neighbouring elements that might be required for binding to Bim1. While in vivo this was sufficient to abrogate the interaction in co-IPs from extracts, we observed that Ase1$^{\Delta N}$ was still able to bind to Bim1 in vitro with no apparently reduced interaction. The in-vitro experiments may not be sensitive enough to detect potential differences in affinities. In living organisms it is often crucial that proteins bind each other just at a given time and that the interactions between them are strictly controlled by regulatory mechanisms like post translational modifications, with phosphorylations being the most prominent one.

In line with this Ase1 and Bim1 are known targets of kinases that regulate their affinity for other proteins [33] [79]. For instance the interaction of Ase1 with Cin8, a kinesin-5 that can slide antiparallel MTs apart is strictly controlled by phosphorylation of Ase1 by Cdk1 (cyclin-dependent kinase) [33]. In metaphase Ase1 is phosphorylated to inhibit its ability to bind Cin8. Premature recruitment of Cin8 by Ase1 at that time would lead to frequent bending and collapse of the metaphase spindle. Later in anaphase Ase1 gets dephosphorylated by Cdc14, a separase-activated phosphatase. This enables the recruitment of Cin8 to the midzone via Ase1, where it is required for spindle elongation [33]. Likewise, Bim1 is phosphorylated by Ipl1p in anaphase, leading to a reduced affinity for static and dynamic MTs [79]. Failures in phosphorylation lead to faster elongating and longer spindles that also show a higher probability of breakage. Moreover, Ipl1, which associates with Bim1 via two SxIP motifs, is a target of the cell cyclin-dependent kinase 1, Cdk1 [84]. Phosphorylation occurs

adjacent to the identified SxIP motifs abolishing premature binding to Bim1. At anaphase onset Ipl1 gets dephosphorylated by the phosphatase Cdc14 and gets recruited to MTs by Bim1 [84].As shown in cells that carry an Ipl1 allele, which cannot be phosphorylated by Cdk1, the premature association of Bim1 and Ipl1 can cause monopolar chromosome segregation and aberrant spindle morphology [84].

It would therefore not be surprising if similar to these highly regulated protein-protein interactions, the association between Ase1 and Bim1 would be tightly controlled in vivo. Live cell imaging might provide an evidence that this is indeed the case. We never observed Ase1 localizing to structures other than the midzone, although Bim1 theoretically should be able to target the protein also to other microtubules, at least in the nucleus. This might indicate the interaction is at least spatially restricted by some mechanisms, maybe by some post translational modifications.

The differences we observe between the in vitro and in vivo pull-downs might result from different posttranslational modifications of the proteins in the experiments. For the in vitro experiments recombinant proteins from bacteria and insect cells were used. These proteins could for instance lack or possess different phosphorylations, which differ from those present in budding yeast at the time when Bim1 and Ase1 interact with each other. The use of proteins purified from yeast cells could provide a solution for that issue. Apart from that, the recombinant proteins could be incubated with the mentioned phosphatases or kinases prior performing the in vitro interaction assays.

Moreover, it cannot be excluded that the in vitro interaction experiments are not sensitive enough to properly detect differences in affinities of Bim1 binding to $Ase1^{\Delta N}$ or $Ase1^{WT}$. Therefore, it might be useful to perform isothermal titration calorimetry with the recombinant proteins to extract accurate dissociation constants.

5.4 Function of the interaction between Ase1 and Bim1 in vivo

So far, the functional role of Ase1 associating with Bim1 in vivo is still an open question. In vitro I could show that the interaction is robust as even in the presence of high ionic strength (300 mM NaCl) a stable complex with a 1:1 stoichiometry was formed. In the performed growth assay the $Ase1^{\Delta N}$ mutant, which shows impaired binding to Bim1, displayed reduced viability in the presence of the microtubule destabilising drug benomyl. This clearly points to a functionally relevant role for the interaction between the two proteins in vivo.

By live cell imaging using endogenously tagged Bim1 in an Ase1 deletion strain I was able to clearly show that Bim1 does not depend on Ase1 for its midzone localization. In contrast to its mammalian homologue, PRC1, which depends on kinesin-4 [109], Ase1 does not require

motor proteins for its midzone localization. Also in cells that are deleted for other known MAPs like Bim1, Fin1, Stu1 and Stu2 no alteration in its localization was found [42].

Although both proteins can clearly independently localize to the midzone, there might be situations, in which the interaction between them might facilitate their proper positioning in cells. In TIRF microscopy Bim1 was able to target Ase1 to individual, non-bundled MTs. Maybe in vivo Bim1 can already recruit Ase1 to MT plus ends prior to their incorporation into the midzone (Fig. 28). The localization to the plus ends of these growing MTs might bring Ase1 in close proximity to its target destination. When the MTs grow past each other, Ase1 would already be perfectly positioned to generate antiparallel bundles. On the other hand, Ase1 could facilitate the association of Bim1 to the spindle midzone after antiparallel MTs have been formed (Fig. 28) leading to a stable pool of Bim1 at the midzone.

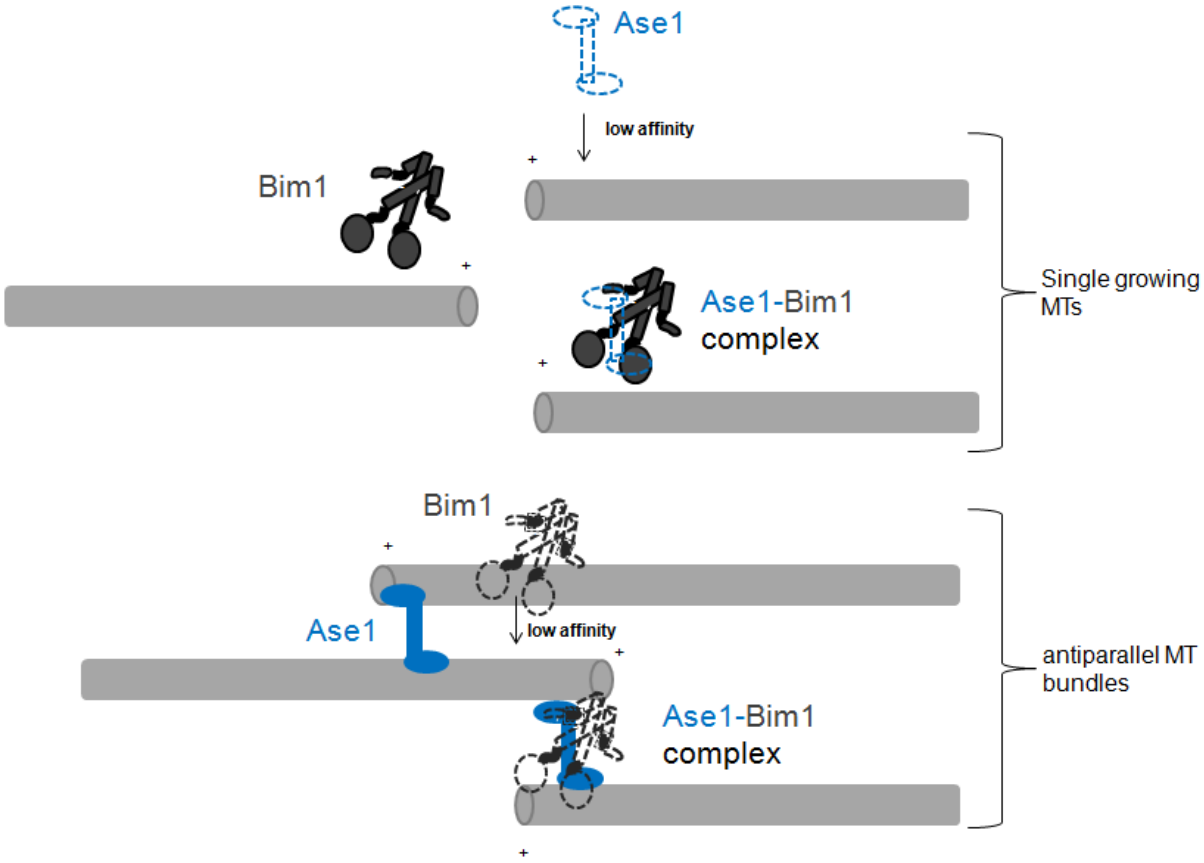

Figure 28. Interplay of Bim1 and Ase1 at the spindle midzone.

Schematic depicts the proposed mechanism by which Bim1 facilitates the localization of Ase1 to the spindle midzone. MTs are shown in light grey, Bim1 in dark grey, Ase1 in blue; proteins displayed by dotted lines have a low affinity for the prevalent form of MTs (single growing MTs or stable antiparallel ones).

In the future it would be useful to carefully investigate by live cell imaging the spindle dynamics in Ase1$^{\Delta N}$ strains. This could shed some light on the role of the interaction in vivo.

Furthermore genetic interactions with other spindle organizers such as the kinesin-5 motors Cin8 and Kip1 or the kinesin-8 depolymerase Kip3 should be tested.

Moreover further TIRF experiments, especially with dynamic MTs, could provide more hints about the functional benefit of the interaction. The TIRF assays done in this study would need to be further optimized. The biggest issue so far seems to be the buffer, with which Ase1 is eluted and stored. Prior to using the protein in TIRF asssays, the buffer should be exchanged by simple dialysis to make it compatible with dynamic microtubule growth and Bim1 end tracking. The problem is that Ase1 tends to form aggregates and pellets rather easily in other buffers like PEM buffer or in a buffer containing 25 mM Hepes pH 8.0 and 150 mM KCl.

Apart from that the TIRF experiments could be further improved by using a recently developed technique called micro patterning [110] [111]. This allows the controlled attachment of MT seeds that serve as nucleation templates onto specific regions. Polyethyleneglycol (PEG)-coated slides are placed under a photomask, which contains transparent spots that form the micropattern of interest. After oxidation of the PEG, induced by deep UV, the exposed sites are competent for MT seeds attachment. Next, free tubulin can be added to allow growth from the seeds. By determining the MT nucleation regions one can significantly higher the probability that MTs grow in an antiparallel position which is crucial for being bundled by Ase1. In this way, a yeast spindle can be constructed and visualized in vitro, which would allow a further investigation of the interplay between Bim1 and Ase1. The fact that EB1 and PRC1 proteins are among the most conserved microtubule regulators, makes a further investigation of their collective behavior crucial for the understanding of microtubule dynamics.

6. Table of figures

Figure 1. Microtubule structure and dynamic instability. 2
Figure 2. PRC1 bundles antiparallel microtubules in the spindle midzone. 5
Figure 3. EB-dimer and its binding partners. 9
Figure 4 Characteristics of the Bim1 binding mutants. 23
Figure 5. Verification of the Bim1 mutants by pulling down known interaction partners. 24
Figure 6. Interaction partners of different N-terminally tagged Bim1 variants. 26
Figure 7. Effects of Bim1 cargo binding mutants on cell viability. 27
Figure 8. Model of $Bim1^{WT}$ binding to its interaction partners and the cargo deficient $Bim1^{YE/AA}$ mutant. 28
Figure 9. Verification of the $Bim1^{YE/AA}$-FLAG mutant by pulling down a known interaction partner. 29
Figure 10. Comparing the interaction partners of $Bim1^{WT}$ and the “cargo deficient” mutant. 30
Figure 11. Testing Bim1 mutants having the known interaction motifs mutated for growth defects. 31
Figure 12. Localization of the Bim1 mutant during Mitosis. 32
Figure 13. Analysis of the spindle orientation defect. 33
Figure 14. Determination of the doubling time of different Bim1 mutants during exponential growth. 34
Figure 15. Testing the interaction between Nup159 and Bim1 variants. 35
Figure 16. Testing the interaction between Bck1 and Bim1. 36
Figure 17. Investigating the interaction between Ase1 and Bim1. 37
Figure 18. Testing the $Ase1^{\Delta N}$ mutant for growth defects. 38
Figure 19. Expression and purification of Ase1 from different organisms. 39
Figure 20. Ase1-STREP binds microtubules in a cosedimentation assay. 40
Figure 21. Ase1 directly interacts with Bim1 via the EBH domain. 41
Figure 22. Size exclusion chromatography analysis of Bim1-Ase1 complexes. 42
Figure 23. Ase1 lacking the N-terminal part shows no reduced binding to Bim1. 43
Figure 24. Bim1-eGFP recruits Ase1-STREP-Alexa594 to taxol stabilized microtubules. 45
Figure 25. In the absence of Bim1, Ase1 preferably associates with bundled microtubules. 46
Figure 26. Investigating the collective behavior of Bim1 and Ase1 on dynamic microtubules. 47
Figure 27. Localization of Bim1. 48
Figure 28. Interplay of Bim1 and Ase1 at the spindle midzone. 54

7. Abbreviations

aa	amino acids
APC	adenomatous-polyposis-coli
bp	base pairs
CAP-Gly	cytoskeleton associated proteins glycine-rich
CH	calponin homology
DMSO	dimethylsulfoxyde
do	dropout
DTT	dithiothreithol
EBH	end binding homology
EDTA	ethylenediamine tetraacetic acid
EGTA	ethylene glycol tetraacetic acid
f.c.	final concentration
FG-repeats	phenylalanine-glycine-repeats
GFP	green fluorescence protein
GMPCPP	guanosine 5'-[α,β-methylene]triphosphate
GST	gluthatione-S-transferase
GTP	guanidine triphosphate
h	hours
HEPES	2-(4-(2-Hydroxyethyl)-1-piperazinyl)-ethansulfonsäure
IPTG	isopropyl-β-D-thiogalactopyranosid
kDa	kilo Dalton
l	Liter
LB	lysogeni broth
MAPs	microtubule associated proteins
max	maximum
min	minutes
ml	milliliter
MT	microtubule
OD	optical density
O/N	overnight
ORF	open reading frame
OS mix	oxygen-scavenger mix
PBS	phosphate buffered saline
PEG	polyethylenglycole
PCR	polymerase chain reaction
PMSF	phenylmethanesulphonylfluoride
rpm	revolutions per minute

rt	room temperature
s	seconds
SDS	sodium dodecyl sulfate
SDS-page	sodium dodecylsulfate polyacrylamide gel electrophoresis
SEC	size exclusion chromatography
SPOC	spindle position checkpoint
TEAB	triethylammonium bicarbonate buffer
TEV	tobacco etch virus
+TIPs	plus-end tracking proteins
TIRF	total internal reflection
UTR	untranslated region
WB	washing buffer
WT	wildtype
w/v	weight/volume
YFP	Yellow fluorescence protein
YPD	yeast extract peptrone dextrose

8. References

1.Ganguly, A., Yang, H., Sharma, R., Patel, K. D. & Cabral, F. The role of microtubules and their dynamics in cell migration. *The Journal of biological chemistry* **287,** 43359-69 (2012).

2.Desai, A. & Mitchison, T. Microtubule polymerization dynamics. *Annual review of cell and* (1997).

3.Burbank, K. S. & Mitchison, T. J. Microtubule dynamic instability. *Current biology : CB* **16,** R516-7 (2006).

4.AMOS, L. & Klug, A. Arrangement of subunits in flagellar microtubules. *Journal of cell science* (1974).

5.Mandelkow, E., Song, Y. & Mandelkow, E. The microtubule lattice—dynamic instability of concepts. *Trends in cell biology* (1995).

6.Sandblad, L., Busch, K., Tittmann, P., Gross, H. & Brunner, D. The Schizosaccharomyces pombe EB1 Homolog Mal3p Binds and Stabilizes the Microtubule Lattice Seam. *Cell* (2006).

7.Vinh, D., Kern, J. & Hancock, W. Reconstitution and characterization of budding yeast γ-tubulin complex. *Molecular biology of* (2002).

8.Burns, R. α- , β- , and γ- tubulins: Sequence comparisons and structural constraints. *Cell motility and the cytoskeleton* (1991).

9.Sirajuddin, M., Rice, L. & Vale, R. Regulation of microtubule motors by tubulin isotypes and post-translational modifications. *Nature cell biology* (2014).
10.Janke, C. & Bulinski, J. Post-translational regulation of the microtubule cytoskeleton: mechanisms and functions. *Nature reviews Molecular cell biology* (2011).
11.Westermann, S. & Weber, K. Post-translational modifications regulate microtubule function. *Nature reviews Molecular cell biology* (2003).
12.Spiegelman, B., Penningroth, S. & Kirschner, M. Turnover of tubulin and the N site GTP in Chinese hamster ovary cells. *Cell* (1977).
13.Wang, H. & Nogales, E. Nucleotide-dependent bending flexibility of tubulin regulates microtubule assembly. *Nature* (2005).
14.Akhmanova, A. & Steinmetz, M. Tracking the ends: a dynamic protein network controls the fate of microtubule tips. *Nature reviews Molecular cell biology* (2008).
15.Drechsel, D. & Kirschner, M. The minimum GTP cap required to stabilize microtubules. *Current Biology* (1994).
16.Mandelkow, E. & Milligan, R. Microtubule dynamics and microtubule caps: a time-resolved cryo-electron microscopy study. *The Journal of cell* (1991).
17.Amos, L. & Schlieper, D. Microtubules and maps. *Advances in protein chemistry* (2005).
18.Dye, R., Fink, S. & Williams, R. Taxol-induced flexibility of microtubules and its reversal by MAP-2 and Tau. *Journal of Biological Chemistry* (1993).
19.Felgner, H., Frank, R. & Biernat, J. Domains of neuronal microtubule-associated proteins and flexural rigidity of microtubules. *The Journal of cell* (1997).
20.Cassimeris, L. & Spittle, C. Regulation of microtubule-associated proteins. *International review of cytology* (2001).
21.Newton, C., Wagenbach, M., Ovechkina, Y. & Wordeman, L. MCAK, a Kin I kinesin, increases the catastrophe frequency of steady-state HeLa cell microtubules in an ATP-dependent manner in vitro. *FEBS letters* (2004).
22.Hunter, A. & Wordeman, L. How motor proteins influence microtubule polymerization dynamics. *Journal of cell science* (2000).
23.Moritz, M. & Da Agard. γ-Tubulin complexes and microtubule nucleation. *Current opinion in structural biology* (2001).
24.Bieling, P., Telley, I. & Surrey, T. A minimal midzone protein module controls formation and length of antiparallel microtubule overlaps. *Cell* (2010).
25.Subramanian, R., Ti, S., Tan, L., Darst, S. & Kapoor, T. Marking and measuring single microtubules by PRC1 and kinesin-4. *Cell* (2013).
26.Subramanian, R. *et al.* Insights into antiparallel microtubule crosslinking by PRC1, a conserved nonmotor microtubule binding protein. *Cell* **142,** 433-43 (2010).

27.Janson, M., Loughlin, R., Loïodice, I., Fu, C. & Brunner, D. Crosslinkers and motors organize dynamic microtubules to form stable bipolar arrays in fission yeast. *Cell* (2007).
28.Tran, P., Marsh, L., Doye, V. & Inoue, S. A mechanism for nuclear positioning in fission yeast based on microtubule pushing. *The Journal of cell* (2001).
29.Lucas, J., Courtney, S. & Hassfurder, M. Microtubule-associated proteins MAP65-1 and MAP65-2 positively regulate axial cell growth in etiolated Arabidopsis hypocotyls. *The Plant Cell* (2011).
30.Mollinari, C., Kleman, J., Jiang, W. & Schoehn, G. PRC1 is a microtubule binding and bundling protein essential to maintain the mitotic spindle midzone. *The Journal of cell* (2002).
31.Schuyler, S., Liu, J. & Pellman, D. The molecular function of Ase1p evidence for a MAP-dependent midzone-specific spindle matrix. *The Journal of cell biology* (2003).
32.Mao, G., Chan, J., Calder, G., Doonan, J. H. & Lloyd, C. W. Modulated targeting of GFP-AtMAP65-1 to central spindle microtubules during division. *The Plant journal : for cell and molecular biology* **43,** 469-78 (2005).
33.Khmelinskii, A., Roostalu, J., Roque, H., Antony, C. & Schiebel, E. Phosphorylation-dependent protein interactions at the spindle midzone mediate cell cycle regulation of spindle elongation. *Developmental cell* **17,** 244-56 (2009).
34.Fu, C., Ward, J., Loiodice, I. & Velve-Casquillas, G. Phospho-regulated interaction between kinesin-6 Klp9p and microtubule bundler Ase1p promotes spindle elongation. *Developmental cell* (2009).
35.Braun, M., Lansky, Z., Fink, G., Ruhnow, F. & Diez, S. Adaptive braking by Ase1 prevents overlapping microtubules from sliding completely apart. *Nature cell* (2011).
36.Subramanian, R. & Kapoor, T. Building complexity: insights into self-organized assembly of microtubule-based architectures. *Developmental cell* (2012).
37.Liu, J. *et al.* PRC1 cooperates with CLASP1 to organize central spindle plasticity in mitosis. *Journal of Biological* (2009).
38.Bratman, S. & Chang, F. Stabilization of overlapping microtubules by fission yeast CLASP. *Developmental cell* (2007).
39.Jiang, W., Jimenez, G., Wells, N., Hope, T. & Wahl, G. PRC1: A Human Mitotic Spindle–Associated CDK Substrate Protein Required for Cytokinesis. *Molecular cell* (1998).
40.Pellman, D., Bagget, M., Tu, Y. & Fink, G. Two microtubule-associated proteins required for anaphase spindle movement in Saccharomyces cerevisiae. *The Journal of cell* (1995).
41.Juang, Y., Huang, J., Peters, J., McLaughlin, M. & Tai, C. APC-mediated proteolysis of Ase1 and the morphogenesis of the mitotic spindle. *Science* (1997).
42.Khmelinskii, A., Lawrence, C. & Roostalu, J. Cdc14-regulated midzone assembly controls anaphase B. *The Journal of cell* (2007).

43.Perez, F., Diamantopoulos, G., Stalder, R. & Kreis, T. CLIP-170 highlights growing microtubule ends in vivo. *Cell* (1999).
44.Scheel, J., Pierre, P. & Rickard, J. Purification and analysis of authentic CLIP-170 and recombinant fragments. *Journal of Biological* (1999).
45.Weisbrich, A., Honnappa, S. & Jaussi, R. Structure-function relationship of CAP-Gly domains. *Nature structural &* (2007).
46.Lansbergen, G., Komarova, Y. & Modesti, M. Conformational changes in CLIP-170 regulate its binding to microtubules and dynactin localization. *The Journal of cell* (2004).
47.Pierre, P., Scheel, J., Rickard, J. & Kreis, T. CLIP-170 links endocytic vesicles to microtubules. *Cell* (1992).
48.Dujardin, D., Wacker, U. & Moreau, A. Evidence for a role of CLIP-170 in the establishment of metaphase chromosome alignment. *The Journal of cell* (1998).
49.Carvalho, P., Gupta, M., Jr, Hoyt, M. & Pellman, D. Cell cycle control of kinesin-mediated transport of Bik1 (CLIP-170) regulates microtubule stability and dynein activation. *Developmental cell* (2004).
50.Sheeman, B., Carvalho, P., Sagot, I., Geiser, J. & Kho, D. Determinants of S. cerevisiae Dynein Localization and Activation: Implications for the Mechanism of Spindle Positioning. *Current Biology* (2003).
51.Akhmanova, A., Hoogenraad, C. & Drabek, K. Clasps are CLIP-115 and-170 associating proteins involved in the regional regulation of microtubule dynamics in motile fibroblasts. *Cell* (2001).
52.Akhmanova, A. *et al.* Clasps are CLIP-115 and -170 associating proteins involved in the regional regulation of microtubule dynamics in motile fibroblasts. *Cell* **104,** 923-35 (2001).
53.Mimori-Kiyosue, Y. & Grigoriev, I. CLASP1 and CLASP2 bind to EB1 and regulate microtubule plus-end dynamics at the cell cortex. *The Journal of cell* (2005).
54.van Breugel, M., Drechsel, D. & Hyman, A. Stu2p, the budding yeast member of the conserved Dis1/XMAP215 family of microtubule-associated proteins is a plus end-binding microtubule destabilizer. *The Journal of cell biology* **161,** 359-69 (2003).
55.Gard, D. L. & Kirschner, M. W. A microtubule-associated protein from Xenopus eggs that specifically promotes assembly at the plus-end. *The Journal of cell biology* **105,** 2203-15 (1987).
56.Severin, F., Habermann, B., Huffaker, T. & Hyman, T. Stu2 promotes mitotic spindle elongation in anaphase. *The Journal of cell biology* **153,** 435-42 (2001).
57.Cassimeris, L. & Morabito, J. TOGp, the human homolog of XMAP215/Dis1, is required for centrosome integrity, spindle pole organization, and bipolar spindle assembly. *Molecular biology of the cell* **15,** 1580-90 (2004).

58.Al-Bassam, J., Larsen, N. A., Hyman, A. A. & Harrison, S. C. Crystal structure of a TOG domain: conserved features of XMAP215/Dis1-family TOG domains and implications for tubulin binding. *Structure (London, England : 1993)* **15,** 355-62 (2007).
59.Brouhard, G. J. *et al.* XMAP215 is a processive microtubule polymerase. *Cell* **132,** 79-88 (2008).
60.Wu, X., Xiang, X. & 3rd, J. A. H. Motor proteins at the microtubule plus-end. *Trends in cell biology* **16,** 135-43 (2006).
61.Gupta, M. L., Jr, Carvalho, P., Roof, D. M. & Pellman, D. Plus end-specific depolymerase activity of Kip3, a kinesin-8 protein, explains its role in positioning the yeast mitotic spindle. *Nature cell biology* **8,** 913-23 (2006).
62.Moore, A. T. *et al.* MCAK associates with the tips of polymerizing microtubules. *The Journal of cell biology* **169,** 391-7 (2005).
63.Jiang, K. *et al.* TIP150 interacts with and targets MCAK at the microtubule plus ends. *EMBO reports* **10,** 857-65 (2009).
64.Beach, D. L., Thibodeaux, J., Maddox, P., Yeh, E. & Bloom, K. The role of the proteins Kar9 and Myo2 in orienting the mitotic spindle of budding yeast. *Current biology : CB* **10,** 1497-506 (2000).
65.Sproul, L. R., Anderson, D. J., Mackey, A. T., Saunders, W. S. & Gilbert, S. P. Cik1 targets the minus-end kinesin depolymerase kar3 to microtubule plus ends. *Current biology : CB* **15,** 1420-7 (2005).
66.Su, L. K. *et al.* APC binds to the novel protein EB1. *Cancer research* **55,** 2972-7 (1995).
67.Askham, J. M., Moncur, P., Markham, A. F. & Morrison, E. E. Regulation and function of the interaction between the APC tumour suppressor protein and EB1. *Oncogene* **19,** 1950-8 (2000).
68.Tirnauer, J. S., O'Toole, E., Berrueta, L., Bierer, B. E. & Pellman, D. Yeast Bim1p promotes the G1-specific dynamics of microtubules. *The Journal of cell biology* **145,** 993-1007 (1999).
69.Mimori-Kiyosue, Y., Shiina, N. & Tsukita, S. The dynamic behavior of the APC-binding protein EB1 on the distal ends of microtubules. *Current biology : CB* **10,** 865-8 (2000).
70.Bieling, P. *et al.* Reconstitution of a microtubule plus-end tracking system in vitro. *Nature* **450,** 1100-5 (2007).
71.Duellberg, C., Fourniol, F. J., Maurer, S. P., Roostalu, J. & Surrey, T. End-binding proteins and Ase1/PRC1 define local functionality of structurally distinct parts of the microtubule cytoskeleton. *Trends in cell biology* **23,** 54-63 (2013).
72.Rogers, S. L., Rogers, G. C., Sharp, D. J. & Vale, R. D. Drosophila EB1 is important for proper assembly, dynamics, and positioning of the mitotic spindle. *The Journal of cell biology* **158,** 873-84 (2002).

73.Tirnauer, J. S., Canman, J. C., Salmon, E. D. & Mitchison, T. J. EB1 targets to kinetochores with attached, polymerizing microtubules. *Molecular biology of the cell* **13,** 4308-16 (2002).
74.Komarova, Y. *et al.* EB1 and EB3 control CLIP dissociation from the ends of growing microtubules. *Molecular biology of the cell* **16,** 5334-45 (2005).
75.Goldspink, D. A. *et al.* The microtubule end-binding protein EB2 is a central regulator of microtubule reorganisation in apico-basal epithelial differentiation. *Journal of cell science* **126,** 4000-14 (2013).
76.Hayashi, I. & Ikura, M. Crystal structure of the amino-terminal microtubule-binding domain of end-binding protein 1 (EB1). *The Journal of biological chemistry* **278,** 36430-4 (2003).
77.Alushin, G. M. *et al.* The Ndc80 kinetochore complex forms oligomeric arrays along microtubules. *Nature* **467,** 805-10 (2010).
78.Maurer, S. P., Fourniol, F. J., Bohner, G., Moores, C. A. & Surrey, T. EBs recognize a nucleotide-dependent structural cap at growing microtubule ends. *Cell* **149,** 371-82 (2012).
79.Zimniak, T., Stengl, K., Mechtler, K. & Westermann, S. Phosphoregulation of the budding yeast EB1 homologue Bim1p by Aurora/Ipl1p. *The Journal of cell biology* **186,** 379-91 (2009).
80.Slep, K. C. *et al.* Structural determinants for EB1-mediated recruitment of APC and spectraplakins to the microtubule plus end. *The Journal of cell biology* **168,** 587-98 (2005).
81.Honnappa, S. *et al.* An EB1-binding motif acts as a microtubule tip localization signal. *Cell* **138,** 366-76 (2009).
82.Jiang, K. *et al.* A Proteome-wide screen for mammalian SxIP motif-containing microtubule plus-end tracking proteins. *Current biology : CB* **22,** 1800-7 (2012).
83.Kumar, P. *et al.* Multisite phosphorylation disrupts arginine-glutamate salt bridge networks required for binding of cytoplasmic linker-associated protein 2 (CLASP2) to end-binding protein 1 (EB1). *The Journal of biological chemistry* **287,** 17050-64 (2012).
84.Zimniak, T. *et al.* Spatiotemporal regulation of Ipl1/Aurora activity by direct Cdk1 phosphorylation. *Current biology : CB* **22,** 787-93 (2012).
85.van der Vaart, B. *et al.* SLAIN2 links microtubule plus end-tracking proteins and controls microtubule growth in interphase. *The Journal of cell biology* **193,** 1083-99 (2011).
86.Mishima, M. *et al.* Structural basis for tubulin recognition by cytoplasmic linker protein 170 and its autoinhibition. *Proceedings of the National Academy of Sciences of the United States of America* **104,** 10346-51 (2007).
87.Peris, L. *et al.* Tubulin tyrosination is a major factor affecting the recruitment of CAP-Gly proteins at microtubule plus ends. *The Journal of cell biology* **174,** 839-49 (2006).
88.Bieling, P. *et al.* CLIP-170 tracks growing microtubule ends by dynamically recognizing composite EB1/tubulin-binding sites. *The Journal of cell biology* **183,** 1223-33 (2008).

89.Vitre, B., Coquelle, F., Heichette, C. & Garnier, C. EB1 regulates microtubule dynamics and tubulin sheet closure in vitro. *Nature cell* (2008).
90.Bieling, P., Laan, L., Schek, H., Munteanu, el & Sandblad, L. Reconstitution of a microtubule plus-end tracking system in vitro. *Nature* (2007).
91.Schwartz, K., Richards, K. & Botstein, D. BIM1 encodes a microtubule-binding protein in yeast. *Molecular biology of the cell* **8,** 2677-91 (1997).
92.Tong, A. H. *et al.* Systematic genetic analysis with ordered arrays of yeast deletion mutants. *Science (New York, N.Y.)* **294,** 2364-8 (2001).
93.Longtine, M. S. *et al.* Additional modules for versatile and economical PCR-based gene deletion and modification in Saccharomyces cerevisiae. *Yeast (Chichester, England)* **14,** 953-61 (1998).
94.Taus, T. *et al.* Universal and confident phosphorylation site localization using phosphoRS. *Journal of proteome research* **10,** 5354-62 (2011).
95.Jain, A., Liu, R., Xiang, Y. K. & Ha, T. Single-molecule pull-down for studying protein interactions. *Nature protocols* **7,** 445-52 (2012).
96.Gouveia, S. M. *et al.* In vitro reconstitution of the functional interplay between MCAK and EB3 at microtubule plus ends. *Current biology : CB* **20,** 1717-22 (2010).
97.Skube, S. B., Chaverri, J. M. & Goodson, H. V. Effect of GFP tags on the localization of EB1 and EB1 fragments in vivo. *Cytoskeleton (Hoboken, N.J.)* **67,** 1-12 (2010).
98.Blake-Hodek, K. A., Cassimeris, L. & Huffaker, T. C. Regulation of microtubule dynamics by Bim1 and Bik1, the budding yeast members of the EB1 and CLIP-170 families of plus-end tracking proteins. *Molecular biology of the cell* **21,** 2013-23 (2010).
99.Lee, L. *et al.* Positioning of the mitotic spindle by a cortical-microtubule capture mechanism. *Science (New York, N.Y.)* **287,** 2260-2 (2000).
100.Miller, R. K., Cheng, S. C. & Rose, M. D. Bim1p/Yeb1p mediates the Kar9p-dependent cortical attachment of cytoplasmic microtubules. *Molecular biology of the cell* **11,** 2949-59 (2000).
101.Wolyniak, M. J. *et al.* The regulation of microtubule dynamics in Saccharomyces cerevisiae by three interacting plus-end tracking proteins. *Molecular biology of the cell* **17,** 2789-98 (2006).
102.Kraemer, D. M., Strambio-de-Castillia, C., Blobel, G. & Rout, M. P. The essential yeast nucleoporin NUP159 is located on the cytoplasmic side of the nuclear pore complex and serves in karyopherin-mediated binding of transport substrate. *The Journal of biological chemistry* **270,** 19017-21 (1995).
103.Lee, K. S. & Levin, D. E. Dominant mutations in a gene encoding a putative protein kinase (BCK1) bypass the requirement for a Saccharomyces cerevisiae protein kinase C homolog. *Molecular and cellular biology* **12,** 172-82 (1992).

104.Hruby, A. *et al.* A constraint network of interactions: protein-protein interaction analysis of the yeast type II phosphatase Ptc1p and its adaptor protein Nbp2p. *Journal of cell science* **124,** 35-46 (2011).

105.Zhu, Z. C. *et al.* Interactions between EB1 and microtubules: dramatic effect of affinity tags and evidence for cooperative behavior. *The Journal of biological chemistry* **284,** 32651-61 (2009).

106.Jaspersen, S. L. & Winey, M. The budding yeast spindle pole body: structure, duplication, and function. *Annual review of cell and developmental biology* **20,** 1-28 (2004).

107.Siller, K. H. & Doe, C. Q. Spindle orientation during asymmetric cell division. *Nature cell biology* **11,** 365-74 (2009).

108.Caydasi, A., Ibrahim, B. & Pereira, G. Monitoring spindle orientation: Spindle position checkpoint in charge. *Cell Div* (2010).

109.Kurasawa, Y., Earnshaw, W. C., Mochizuki, Y., Dohmae, N. & Todokoro, K. Essential roles of KIF4 and its binding partner PRC1 in organized central spindle midzone formation. *The EMBO journal* **23,** 3237-48 (2004).

110.Portran, D., Gaillard, J., Vantard, M. & Thery, M. Quantification of MAP and molecular motor activities on geometrically controlled microtubule networks. *Cytoskeleton (Hoboken, N.J.)* **70,** 12-23 (2013).

111.Su, X. *et al.* Microtubule-sliding activity of a kinesin-8 promotes spindle assembly and spindle-length control. *Nature cell biology* **15,** 948-57 (2013).

112.Ashford, A. *et al*. Preparation of tubulin from bovine brain. *Cell Biology: A Laboratory Handbook. Academic Press*, pp. 205–212 (1998)

Curriculum Vitae

Contact information

Name:	Fischböck Josef
Address:	Fruchtgasse 3/13 1020 Vienna
Cell Phone:	06802384755
Email:	Josef_Fischboeck@hotmail.com

Personal information

Nationality:	Austria
Date of Birth:	02.03.1988
Place of Birth:	Vöcklabruck

Education

2006	Matura, BRG Gmunden
2007 – 2008	Biomedical engineering, FH Technikum Vienna
2008 – 2011	Bachelor of Science Biology (elective module: microbiology and genetics), University of Vienna
From Oct. 2011	Master Molecular biology (elective module: biochemistry), University of Vienna

Research experience

Internships:

Max F. Perutz Laboratories, Vienna, laboratory of Dr. Silke Dorner, Supervisor Sanja Antic, MSc, July-August 2012

Max F. Perutz Laboratories, Vienna, laboratory of Prof. Andreas Bachmair, Supervisor Supervisor Konstantin Tomanov, MSc, November-December 2012
"The role of functional domains in the SUMO ligase PIAL2"

Institute of Molecular Pathology (IMP), Vienna, laboratory of Dr. Stefan Westermann, Supervisor Dr. Babet van der Vaart, March-May 2013

Master-thesis:

Institute of Molecular Pathology (IMP), Vienna, laboratory of Dr. Stefan Westermann, Supervisor Dr. Babet van der Vaart, May 2013- August 2014
"Exploring the molecular basis for different EB1 interaction networks in budding yeast"